CO_2-Corrosion of Carbon steel: The Synergy of Chloride Ion Concentration and Temperature on Metal Penetration.

Frederick Pessu, Richard Barker and Anne Neville.

Article history: (This style is Article Info subhead)

Received Day Month Year (This style is Article History and Keywords)
Accepted Day Month Year
Available Day Month Year

Keywords: (This style is Article Info subhead)

A. Carbon dioxide
C. Carbon steel
D. Ferrite
E. General corrosion
F. Pitting
G. Pitting factor

Institute of Functional Surfaces (iFS), School of Mechanical Engineering, University of Leeds. Leeds. United Kingdom. LS2 9JT.

***Dr Frederick Pessu: Email: (f.o.pessu@leeds.ac.uk).

ABSTRACT

This paper investigates the synergy of chloride ion concentration and temperature on the general and pitting corrosion of carbon steel in CO_2 saturated environments. Experiments were conducted over 168 h in different concentrations of NaCl brines (1, 3.5 and 10 wt. %) and temperatures (30, 50 and 80°C) with the aim of elucidating the combined effect of changes in chloride ion concentration and temperature on overall metal degradation; taking into consideration general and pitting corrosion. This also includes a correlation with the formation and properties of $FeCO_3$ corrosion products. Linear polarisation resistance (LPR) was implemented to monitor the electrochemical responses. Corrosion product characteristics and morphologies were studied through a combination of scanning electron microscopy (SEM) and X-ray diffraction (XRD). Pitting corrosion evaluation was conducted through the application of 3D surface profilometry to study pit geometries such as the depth and diameter. The results show that general and pitting corrosion is strongly correlated to the synergistic effects of changing chloride ion concentration and temperature in carbon steel as a result of their combined influence on ferrite (Fe) dissolution and $FeCO_3$ formation. This represents a paradigm shift from the already established mechanisms on chloride ion and temperature effects on passive alloys such as stainless steel. Increasing chloride ion concentration and temperature up to 10 wt. % NaCl and 50-80°C, respectively is observed to increase the rate of Fe dissolution and formation of semi-protective $FeCO_3$ corrosion products, leading to the increase manifestation and severity of pitting corrosion. The results also show a "threshold chloride concentration" exists at 30°C, above which there is no significant increase in corrosion rate. However, such "thresholds effect" were not observed at higher temperatures evaluated in the range of chloride concentration considered in this study.

INTRODUCTION

Corrosion of pipeline steel in oilfields is usually characterized by a complex material degradation mechanism. In most oilfield scenarios, the corrosion damage mechanisms often experienced are driven by synergistic interactions of various process parameters, especially in its applications in CO_2 and/or H_2S-saturated environments. Corrosion damage in such environments is usually dominated by, but not limited to general and/or pitting corrosion[1]. Chloride ions have been considered as an important environmental parameter that can affect the process of pitting corrosion of carbon steels in oilfields by destabilising the characteristic protectiveness of a $FeCO_3$ corrosion product[2, 3]. Incidences of a combination of pitting and general corrosion failures in CO_2-saturated environment are presently of significant concern[4]. This is because of the lack of fundamental understanding of localized/pitting corrosion components in the degradation process of carbon steels in such environments, and the difficulty associated with predicting the dominant nature and risks of localized and/or pitting corrosion of carbon steels.

For active materials such as carbon steel, the prospect of significant general corrosion makes the mechanism of pitting corrosion complex, as both corrosion process are capable of occurring at the same time on a particular region of pipeline steel. Some of these complexities are possibly linked to the contributing driving force for general and pitting corrosion of carbon steels in these environments [5-7]. In such environments, the ionic strength contribution of dissolved chloride ions in the brine phase is also important[8]. It has been reported that the pitting corrosion process of carbon steel in CO_2 environments is driven by localized breakdown of protective and/or formation of a non-protective $FeCO_3$[9, 10]). It has also been shown in previous publications[6, 11] and by the work of other authors[7, 12], that factors such as temperature, pH, and exposure time can influence the CO_2 corrosion process, associated film formation characteristics and morphology. These factors could also influence the tendency for pitting corrosion of carbon steel to occur in these environments.

Water chemistry is considered one of the most influential parameters affecting CO_2 corrosion. The mechanism of CO_2 corrosion is known to be dependent on many interrelated physicochemical factors whose interactions with steel in CO_2-saturated environments is considered very important[13]. Oilfield produced water is usually characterized by a high amount of dissolved salts, with chloride ions being the most prominent [14-16]. The role of dissolved chloride in accelerating corrosion reactions[13], and hence pitting corrosion of passive alloys such as stainless steel are already widely recognized[15]. For stainless steels, chloride ion concentration in the solution is considered as a decisive parameter in defining the pitting resistance of stainless steel[15]. The autocatalytic process of pit propagation in stainless steels is known to be driven by chloride ions[17] acting to reduce the local pH and prevent the re-passivation of active pits.

In carbon steel, chloride ions have been reported to be more aggressive than other halides because of their smaller atomic diameter, and as such can fundamentally be considered as an aggressive agent of corrosion capable of destabilising corrosion product layers [2, 13, 16]. However, the mechanism by which this effect is manifested in carbon steel has also remanined elusive. There is a significant lack of understanding of the role of chloride ion concentration on pitting corrosion of carbon steel where there is significant contribution of general corrosion. Most existing models of the effect of chloride ion across various temperature ranges in carbon steel corrosion is still built on established understaning of the effect of chloride ion on passive alloys. The most recent studies

on this subject have consistently offered conflicting viewpoints while mostly focusing exclusively on general corrosion. There has been little or no attention to the effect of chloride ion on the combined evolution of general and pitting corrosion of carbon steel.

Experiments by Luo and Singh[8] on carbon steel in simulated fuel-grade ethanol (SFGE) show an increase in corrosion rate with increasing chloride ion from 0 to 160 mg/L of NaCl at room temperature. This trend is also consistent with similar observations reported by Papavinasam et al[9], who varied chloride ion concentration from 10,000 ppm to 120,000 ppm (other operational variables associated with these experiments were not disclosed). Contrasting viewpoints were present from experiments by Jiang et al[18] at 80°C, Fang et al[19] at 25°C and da Chagas Almeida[20] at 24˚C. All three authors concluded that corrosion rate decreases with increasing chloride ion concentration, while Jiang et al[18] and Fang et al[19] suggested that the risk of pitting corrosion decreases with increase in chloride ion concentration. However, Fang et al[19] also suggested that the presence of chlorides gave an indication of an increase in solution conductivity and ionic strength, but stops short of confirming a possible effect of lower solution resistance (linked to solution conductivity/ionic strength) on the general corrosion rate.

A recent study by Gao et al[2] also reported on the destructive capabilities of increasing chloride ion on pre-formed $FeCO_3$ at 80°C. Changes in chloride ion were achieved in this study by the introduction of $NaClO_4$ into a corrosive environment after the formation of protective $FeCO_3$. The result from this study shows that Cl^- ion and/or ionic strength can destabilize an already formed protective corrosion product layer leading to pit initiation. However, it does not explain the evolution of the pitting process with consideration for the general corrosion process that supports pitting corrosion and drive metal penetration for carbon steel materials[6].

The work presented in this paper is focused on understanding how changes in chloride ion concentration in combination with changes in temperature can influence the corrosion mechanisms and characteristics of carbon steels in an unbuffered CO_2-saturated environment. This study aims to elucidate the synergy of two critical environmental variables; temperature and chloride ion concentration on the general and pitting corrosion process of carbon steels in CO_2 environments.

Materials and Experimental Procedure

The purpose of this work is to investigate the general and localized corrosion processes of carbon steel in three different CO_2-saturated environments, containing 1, 3.5 and 10 wt. % NaCl, each at temperatures of 30°C, 50°C and 80°C. The focus of this study is to understand how general corrosion (related to ferrite dissolution), $FeCO_3$ formation and pitting corrosion processes of carbon steel are influenced by changes in chloride ion concentration in synergy with temperature. The partial pressure of CO_2 gas in the gas phase of the corrosion environment at different temperature are provided in Table 1

Materials: X65 carbon steel samples were used as the working electrodes within a three-electrode cell in each experiment. The steel is composed of a ferritic/pearlitic microstructure. The nominal composition of X65 steel is provided in Table 2.

The carbon steel was sectioned into 10 mm x 10 mm x 5 mm samples. Wires were soldered to the back of each test specimen and then embedded in a non-conducting resin. Prior to the start of each experiment, test samples were wet-ground up to 1200 silicon carbide grit paper, degreased with acetone, rinsed with distilled water and dried with compressed air before immersion into the test brine. A surface area of 1 cm^2 was exposed to the electrolyte per sample and 10 samples were immersed in each 2 litre vessel.

Brine preparation and test conditions: Three different NaCl brine solutions were used for all experiments. The test solution was saturated with CO_2 for a minimum of 12 h (usually overnight) prior to starting each experiment to deaerate the test environment. CO_2 was also bubbled into the system throughout the duration of every test and all tests were conducted at atmospheric pressure. The experiment matrix is shown in Table 3.

In-situ electrochemical measurements: Twin test cells were used in each experiment to ensure repeatability of corrosion rate measurements. Corrosion rates were recorded from two samples per test cell. 10 samples, each of 1 cm^2 surface area, were immersed into a 2 litre test solution. The samples used for monitoring electrochemical responses remained inside the test cells until the end of the experiment to allow full collection of electrochemical data over the 168 h. Corrosion rate measurements were conducted using both DC and AC measurements with an ACM potentiostat. DC Linear polarisation resistance (LPR) measurements were performed by polarising the working electrode ±15 mV about the open circuit potential (OCP) at a scan rate of 0.25 mV/s to obtain polarisation resistance measurements (R_p). Tafel polarisation measurements were performed on freshly ground samples in separate tests to determine anodic and cathodic Tafel constants. This was combined with Faraday's Law and the measured values of R_p to estimate general corrosion rates. Tafel plots were obtained by performing anodic and cathodic sweeps ±250 mV about the OCP at a scan rate of 0.25 mV/s. Both anodic and cathodic sweeps were performed on separate samples in the same test vessel to ensure reliable measurements. Tafel polarisation measurements were performed after 7 h in separate experiments to those samples from which corrosion measurements were recorded over 168 h. Electrochemical impedance spectroscopy measurements were made to account for solution resistances. To ensure that the measured solution resistance truly reflects the ionic strength of electrolyte, the proximity between reference, counter and working remained consistent in each test and for the duration of the tests. This was achieved by adding the samples through designated holes to ensure that all working electrodes are equidistant from the reference electrode, especially the sample used for electrochemical measurements.

Characterisation of $FeCO_3$ corrosion products and pitting corrosion: Corrosion tests were conducted for 168 h with the aim of monitoring the changes in different morphologies of corrosion products and assessing their influence on the evolution of general corrosion and the surface pitting at chosen test conditions. Corrosion product characterisation was performed using Scanning Electron Microscopy (SEM) and X-ray Diffraction (XRD). XRD patterns were collected using a Bruker D8[1] equipped with a LynxEye[2] detector, using a 90 position auto sampler and employing Cu Kα radiation with an active area of 1cm^2 programmable di-vergence slits. Scans were performed over a range 2Θ = 10 to 70° at a step size of 0.033 per second and a total scan time of

[1] Trade name

[2] Trade name

~50 minutes. The results were analysed using X'Pert [3] HighScore software and compared with individual crystal standards from an in-house database.

Surface profilometry was implemented in this study to quantify pitting attack. Samples removed at different time intervals from the same test conditions were cleaned to remove all traces of corrosion products using Clarke's solution before using profilometry to determine the extent of pitting corrosion on the steel surface. Clarke's solution consisted of 20 g antimony trioxide + 50 g stannous chloride + 1000 ml 38% hydrochloric acid, prepared in accordance with ASTM[4] Standard G1-03. The sample surfaces were wiped with a cotton pad soaked in Clarke's solution, washed, air dried, and carefully stored in a de-aerated chamber to avoid oxidation prior to surface analysis. Pit depth measurements were performed in alignment with ASTM standard G46-94[21]. NPFLEX[5] 3D interferometer was used for obtaining the discrete geometry of pits on over 81% of the steel surface (the remaining 19% represents the edges of the sample) to represent the entire exposed surface area. Pits were identified based on carefully chosen thresholds. The thresholds were chosen with reference to the surface roughness of generally corroded areas surrounding the pits. This enabled pits with distinct pit parameters of interests; pit-mouth diameters and pit depths, to be identified and quantified. ASTM G46-94 stipulates that an average depth of the 10 deepest pits and the depth of deepest pit (based on relative pit depth measurement after removal of corrosion products) should be used for evaluating and quantifying the extent of pitting corrosion damage. The measured pits are ranked according to how deep they are across the entire exposed surface. The 10 deepest are used to calculate the average pit depth for a specific test condition, according to ASTM standard G46-94[21]. This is plotted along with the depth of the deepest pit identified. On the basis of the recommendation in the ASTM standard G46-94[21], the pit density was not quantified in this study.

Results and Discussion

Stern-Geary constants were calculated using condition specific Tafel constants from polarisation measurements for carbon steel in three different chloride concentrations at each temperature. The Stern-Geary constants are provided in Solubility data for dissolved CO_2 (Table 3) is calculated using experimentally determined Henry's coefficients for CO_2 in water at different NaCl solutions and at different temperatures by Zheng et al.[37].

Table 4. Stern-Geary constants (B) were used in Equation 1 to calculate corrosion current and consequently corrosion rate based on a total exposed projected surface area of 1 cm^2 per sample.

$$i_{corr} = \frac{1}{2.303R_p}\left[\frac{1}{\beta_a} + \frac{1}{\beta_c}\right]^{-1} = \frac{B}{R_p} \qquad \textbf{Equation 1}$$

Note: the corrosion rate estimated from linear polarisation (LPR) measurements captures both the material loss responses occurring across the entire exposed surface including the localized regions. Therefore it is not used as a true quantitative measure of contribution of general and pitting corrosion in this study. However, the trend in LPR responses (in the form corrosion rate) gives an indication to the extent to which corrosion products is being deposited on the steel surface to impede corrosion process. It is important to note that corrosion product established as a result will also occur at areas where pitting corrosion is likely to manifest.

Corrosion rates and ferrite dissolution

Corrosion rate calculated from LPR measurements and measured *in-situ* pH of the bulk solution are presented in Figure 1(a) and (b), Figure 2(a) and (b) and Figure 3(a) and (b) for 30, 50 and 80°C, respectively. In Figure 1(a), the first 24 h shows approximately equal corrosion rate of ~1.1 mm/yr for tests in 1 and 10 wt. % NaCl at 30°C, and a slightly higher corrosion rate for test in 3.5 wt. % NaCl at ~1.5 mm/yr. This observation indicates a "threshold effect" which can be linked to the "salting out effect" of chloride concentration on dissolved CO_2 gas[3] (provided in Table 3). Decreasing dissolved CO_2 with increasing chloride concentration reduces the driving force for the cathodic reaction[1]. Salting-out effect describes the decrease in solubility due to the presence of a salt in a solute-solvent system[3]. However, increase in the ionic strength and hence the conductivity of the electrolyte due to higher chloride concentration could also offer a counter effect of increase in corrosion rate. This could be the reason why initial corrosion rate is higher in 3.5 wt. % NaCl. At low temperature (30°C) and atmospheric pressure, it is believed that the "salting out effect" of NaCl on dissolved CO_2 is more dominant than the electrolyte conductivity effect[3], especially in the initial stages of the corrosion process. Electrolyte conductivity is related to the rate of transfer of electrons. Other researchers [3, 13, 22] have also reported on the threshold effect at lower temperature. According to Fang et al.[22], at 20°C and after 24 h, corrosion rate decreases by 50% with increase in chloride concentration from 3 to 10 wt.%, which is similar to results shown in Figure 1(a) after 24 h. Eliyan et al.[13] reported an increase in corrosion rate with increase in chloride concentration in terms of NaCl from 0 to 1.5 wt.% at 20°C, after which the corrosion rate decreases steadily to 3.5 wt.% concentration and remained constant up to a concentration of 8 wt.%, while Liu et al.[23], observed peak corrosion rate at 2.5 wt. % of Cl^- concentration for tests carried out between 0-15 wt. % Cl^- at 2 MPa, 100˚C for 72 h in CO_2 saturated systems. Within the same 24 h period, there is no evidence of "threshold effect" with respect to chloride concentration as shown in Figure 2(a) and Figure 3(a) for tests at 50 and 80°C respectively. The absence of the threshold effect is due to the dominance of the ionic strength and hence the electrolyte conductivity effect of the environment on the redox charge exchanges that drives ferrite dissolution and corrosion process at high temperature. Referring to Table 3, the salting effect on dissolved CO_2 is significant. However, at high temperatures, this is suppressed and the increased aggressiveness of the corrosion environment represents a synergy of chloride concentration and temperature on the corrosivity of water chemistry [8, 16, 24].

According to Figure 1(a), the "threshold effect" disappears at 30°C after 24 h, resulting in a continuous increase in corrosion rate in 10 wt.% NaCl until an equal corrosion rate is attained for tests in in 3.5 and 10 wt.% NaCl. The change in the corrosion rate profile between 24-168 h now follows an expected trend of increased solution conductivity and aggressiveness (decreasing solution resistance); also reported by Fang et al[19], with increase in chloride concentration (measured solution resistances were 27.5±0.5 ohms.cm^2, 9.0±0.2 ohms.cm^2 and 4.1±0.2 ohms.cm^2 for 1, 3.5 and 10 wt.% NaCl, respectively at 30˚C from this study). With respect to increasing aggressiveness of corrosion environments, it is expected that charge-transfer will increase, leading

[3] Trade name

[4] Trade name

[5] Trade name

to increasing corrosion rate as shown in the later stages of corrosion rate in **Error! Reference source not found.**(a). While the time-dependent disappearance of the "threshold effect" remains unclear, it is believed that the overall corrosion rate behavior is the result of the competitive effect of "salting out effect" on dissolved CO_2 and aggressiveness of the corrosion environment and potentially other secondary effects that have not been considered in this study. The work by das Chagas Almeida et al[20] at CO_2 partial pressure of 100 kPa and 30 MPa distilled water and 18.7 wt.% NaCl (3.2M NaCl) at 24˚C shows that at higher pressure, the corrosion rate was higher with high NaCl. This is also an evidence to support the findings in the paper that the "threshold effect" is limited by a range of other environmental parameters within a corrosion system. It is important to note that the results of Fang et al.[22] and Liu et al.[23] were based on a 24 h and 72 h exposure, respectively, while the exposure time for the experiment by Eliyan et al[13] was not stated.

The corrosion rate measured for the tests conducted at 50 and 80˚C was consistent throughout the duration of the experiments (see Figure 2(a) and Figure 3(a) for 50 and 80˚C, respectively), showing strong direct correlation with increase in aggressiveness of environment. The solution resistance of corrosion environment at 80°C was measured at 14.8±0.2 ohms.cm^2, 4.9±0.6 ohms.cm^2 and 2.6±0.0 ohms.cm^2 for 1, 3.5 and 10 wt. % NaCl, respectively. This is significantly higher than at lower temperatures (30°C). This observation indicates the effect of thermal activation of chloride ions at corrosion interfaces at high temperatures[16], leading to higher rates of ferrite dissolution. The difference in the corrosion behaviour at 50 and 80°C is primarily in terms of the magnitude of the corrosion rate and the time it takes to peak corrosion rate values. Such difference clearly highlights the synergy of chloride ions and temperature in driving the Fe dissolution process. Corrosion rate peaked within the first 11 h (at ~ 3.2mm/yr, 5.6 mm/yr and 7.0 mm/yr) for tests in 1, 3.5 and 10 wt. % NaCl at 80°C and within the first 60 h (at ~ 2.2mm/yr, 3.5 mm/yr and 5.3 mm/yr) for tests in 1, 3.5 and 10 wt. % NaCl at 50°C. The relatively faster rate to peak corrosion rate and reduction of corrosion rate with time observed at 80˚C than at 50 and 30°C can be attributed to the rate of Fe^{2+} generation from Fe dissolution and saturation of corrosion interface for $FeCO_3$ formation[9] (although amorphous in nature and semi-protective due to the relatively low but continuously evolving pH (shown in Figure 1(b), Figure 2(b) and Figure 3(b) for 30, 50 and 80°C, respectively)). This is discussed in detail in the next section.

Corrosion product formation

The effect of chloride concentration and temperature on the formation and evolution of corrosion product layers is shown by the SEM images provided in Figure 4, Figure 6 and Figure 8 for 30, 50 and 80°C respectively and the XRD patterns in Figure 5, Figure 7 and Figure 9 for 1 and 10 wt.% NaCl solutions at for 30, 50 and 80°C, respectively. Before discussing the corrosion product formation process in detail, it is important to establish the relationship between Fe dissolution, $FeCO_3$ formation and *in-situ* pH changes with time shown in Figure 1(b), Figure 2(b) and Figure 3(b) for 30, 50 and 80°C, respectively. It is believed that the reduction of corrosion rate is due to the formation of corrosion products, specifically $FeCO_3$. However, the extent of such reducing effect is determined by the competing effect of rate of release of Fe^{2+} and $FeCO_3$ formation at the corrosion interface and correlated to evolving bulk and surface pH[25]. According to Guo et al.[25], increasing *in-situ* pH is an indication that the rate of Fe dissolution is greater than the rate of precipitation of $FeCO_3$. *In-situ* pH will remain constant or decreases when the rate of Fe dissolution equals or is lower than the rate of $FeCO_3$ precipitation[25]. Increase in Fe dissolution removed more H^+ from the environment, creating a charge imbalance. H^+ removed by the cathodic reaction is replenished by H_2CO_3 acting as a buffer. The balance of rate of removal of H+ and replenishment by H_2CO_3 could either increase or decrease the pH depending on the direction of change of charge neutrality. Of all the pH data shown in Figure 1(b), Figure 2(b) and Figure 3(b) for 30, 50 and 80°C respectively, a period of constant pH is established to confirm the scenario of equal rate of Fe dissolution and $FeCO_3$ formation except for test in 10 wt. % NaCl at 80°C. Prior to the end of the test in 10 wt. % NaCl at 80°C, there was an initial increase in pH from ~3.9 at the start to ~5.6 after 50 h, corresponding to periods of increasing Fe dissolution and followed by a drop in pH after ~50 h. This is attributed to the scenario where the rate of precipitation of $FeCO_3$ becomes greater than the rate of generation of Fe^{2+}[25]. It also indicates attainment of saturation of the corrosion interface far above the saturation limit for $FeCO_3$. This scenario was only observed in the case of 10 wt. % NaCl at 80°C and not at lower concentration of NaCl and/or lower temperatures. This is a direct effect of the aggressiveness of the environment to drive Fe dissolution process, $FeCO_3$ formation, thus, confirming the synergy of chloride ions and temperature. It is also important to note that the results presented in Figure 1(b), Figure 2(b) and Figure 3(b) for 30, 50 and 80°C respectively in this study and the observation in Guo et al[25] are based on experiments in closed systems. In such systems the exchange of interfacial ionic species for $FeCO_3$ with the bulk environment is limited and hence rate of saturation of the interface can be directly correlated to the rate of Fe dissolution with the consequence of inducing real-time buffering effect on the bulk pH shown in Figure 1(b), Figure 2(b) and Figure 3(b). It is believed that in actual oilfield pipe interfaces, mass transfer effect will likely be substantial leading to a different effect of Fe dissolution on changes in in-situ pH. Particularly as mass transfer effect will remove Fe^{2+} from the interface while also replenishing the aggressive ions that drives Fe dissolution. Thus it is likely that longer exposure time will be required to achieve similar bulk pH changes observed in this study. In some cases this may only occur during pipe shut-in or in the event of restriction to pipe flow.

From the SEM images in Figure 4, Figure 6 and Figure 8 for 30 (after 168 h), 50 (after 7 and 168 h) and 80°C (after 7 and 168 h), respectively, it is evident (especially from Figure 6(a)-(f) and Figure 8(a)-(f) for tests at 50 and 80°C after 7 and 168 h) that the formation of $FeCO_3$ is usually preceded by Fe dissolution, leaving behind an iron carbide (Fe_3C) network[1, 5, 6, 26]. There is also evidence of a polycrystalline form of $FeCO_3$ after 168 h ($FeCO_3$ was identified using XRD as shown in Figure 5, Figure 7 and Figure 9 for test at 30, 50 and 80°C respectively in 1 and 10 wt. % NaCl solutions). The nature of $FeCO_3$ formed across the three temperatures of interest after 168 h shows a transition from amorphous and/or polycrystalline to crystalline $FeCO_3$ in the direction of increase in both temperature and chloride concentration. At each temperature, the transition from amorphous and/or polycrystalline to crystalline $FeCO_3$ also occurs in the direction of increasing chloride concentration. This is most evident for test in 10 wt. % NaCl; Figure 4(c), Figure 6 (f) and Figure 8 (f) for 10 wt. % at 30, 50 and 80°C, respectively. These observations correlate with the trend of increase in high initial corrosion rate (Fe dissolution) due to the aggressiveness (presence of chloride ion at high temperatures) of the environment. This same aggressiveness is driving the evolution of $FeCO_3$ from an amorphous and/or polycrystalline to easily identifiable $FeCO_3$ crystals. XRD patterns shown in Figure 5, Figure 7 and Figure 9 for test at 30, 50 and 80°C, respectively in 1 and 10 wt. % NaCl solutions consistently show an increase in the intensity of peaks for $FeCO_3$ with increase in chloride ion concentration. This is a direct correlation between progressive increase of Fe dissolution (related to

increased corrosion rate) with the morphology of $FeCO_3$ corrosion product and the transition from amorphous and/or polycrystalline to crystalline $FeCO_3$ over 168 h. It is therefore evident that in an unbuffered and closed corrosion system and in the absence of any pre-formed $FeCO_3$ (typical for new oilfield flow lines), the effect of chloride concentration is strongly associated with its influence on the electrolytic strength and aggressiveness of the corrosion environments. This also imply that $FeCO_3$ film formation can also be enhanced with increase in chloride ion concentration by the same mechanism, leading to increase in the interfacial saturation level for formation of $FeCO_3$[5]. This effect is shown in this study to be further enhanced by increase in temperature via thermal activation of chloride ion [16, 27]. Increasing temperature accelerates most of the chemical, electrochemical and transport processes at the corrosion interface; H^+ reduction and H_2CO_3/HCO_3^- reduction (or its buffering effect)[28, 29]. Thermal activation of chlorides ions at higher temperatures therefore impacts the rate of electrochemical activation of carbon steel to lose more Fe^{2+} and as shown by the results in this study also contributes towards the precipitation of $FeCO_3$[16, 27]. These trends represents the synergy that exist between temperature and chloride ion concentration in terms of metal penetration from general corrosion rate and rate of saturation of corrosion interface. This synergy is summarised in Figure 10 in terms of the estimated thickness loss due to general corrosion from LPR measurements after 72 and 186 h. Estimated thickness loss presented in Figure 10 is based on LPR measurements on the assumption that corrosion rate captured from the electrochemical measurement is general across the entire corrosion interface. Although this could also takes into account the localized electrochemical activity related to pitting corrosion, it provides a useful baseline for qualifying the aggressiveness of the bulk environment and its transition with time. The pitting corrosion contribution to LPR measurement is assumed to be relatively small in comparison to the general corrosion process taking place across the entire surface. This is evident from the data on estimated thickness and the pitting corrosion analysis presented later in this paper.

The results reported thus far in this paper is in contrast to the general viewpoints on the influence of chloride ion on the process of corrosion product formation by several authors [2, 16, 30]. Chloride ions have often been linked to the destabilisation of $FeCO_3$ corrosion products; after it is formed, and increasing the solubility product and saturation limit required for the formation of $FeCO_3$ corrosion products. It is important to note that in the findings of Gao et al[2] that also support this viewpoint, $FeCO_3$ corrosion products were initially formed at a high initial pH of 6.6 and Fe^{2+} concentration of 100 ppm in a 0.1-1 wt. % NaCl solution before subjecting the corrosion media to higher chloride ion concentration. While the work of Gao et al[2] may have shown that higher chloride ion concentration could destabilise the corrosion products, the results presented in this work provides useful understanding of the effect of chloride ion concentration on Fe dissolution and $FeCO_3$ corrosion product evolution in CO_2 corrosion systems. The result presented here is particularly relevant for CO_2 saturated corrosion environments where the corrosion product formation process is slowly preceded by electrochemical dissolution of Fe^{2+} as shown by the results Figure 6 and Figure 8 at 50 (after 7 and 168 h) and 80°C (after 7 and 168 h), respectively.

Pitting corrosion

The results discussed in this section is focused on the relationship between pitting corrosion of carbon steel and the synergetic influence of chloride ion concentration and temperature. This is also discussed in the context of overall metal penetration. The depth of the deepest pit, average depth of pit and the aspect ratio based on the deepest pit on ~81% of the entire exposed 1 cm^2 sample over 168 h for different chloride concentration are provide in Estimated thickness loss (µm) based on LPR measurements showing the synergistic effect of chloride ion concentration and temperature on carbon steel penetration after (a) 72 h and (b) 168 h. *Note: severity of material loss in magnitude increases in this order; Green → Amber → Red.*

Figure 11, Pitting corrosion in X65 carbon steel in different NaCl solutions over 168 h, at 30°C (a) Deepest pit, (b) average depth of pits and (c) Aspect ratio based on the diameter of deepest pit. *Note: Pit depth quantified after removal of corrosion product layer and Error bars on average depth of pits represents the standard deviation of 10 deepest pits*

Figure 12 and Pitting corrosion in X65 carbon steel in different NaCl solutions over 168 h, at 50°C (a) Deepest pit, (b) average depth of pits and (c) Aspect ratio based on the diameter of deepest pit. *Note: Pit depth quantified after removal of corrosion product layer and Error bars on average depth of pits represents the standard deviation of 10 deepest pits.*

Figure 13 for 30, 50 and 80°C, respectively. Since the depths of pits are characterized after removal of corrosion products, it is important to note that the contribution of Fe dissolution to metal penetration is already removed in the data shown in Estimated thickness loss (µm) based on LPR measurements showing the synergistic effect of chloride ion concentration and temperature on carbon steel penetration after (a) 72 h and (b) 168 h. *Note: severity of material loss in magnitude increases in this order; Green → Amber → Red.*

Figure 11, Pitting corrosion in X65 carbon steel in different NaCl solutions over 168 h, at 30°C (a) Deepest pit, (b) average depth of pits and (c) Aspect ratio based on the diameter of deepest pit. *Note: Pit depth quantified after removal of corrosion product layer and Error bars on average depth of pits represents the standard deviation of 10 deepest pits*

Figure 12 and Pitting corrosion in X65 carbon steel in different NaCl solutions over 168 h, at 50°C (a) Deepest pit, (b) average depth of pits and (c) Aspect ratio based on the diameter of deepest pit. *Note: Pit depth quantified after removal of corrosion product layer and Error bars on average depth of pits represents the standard deviation of 10 deepest pits.*

Figure 13. The diameter of the deepest pit for 1 and 3.5% wt. NaCl at 30, 50 and 80°C were used in combination with the depth of deepest pit to estimate the aspect ratio. The aspect ratio is defined as the ratio of the diameter ($Dia._{max}$) and depth (d_{max}) of the deepest pit on an entire exposed surface area. It is mathematically presented in Equation 2. It highlights the role and scope of influence of general corrosion in the pitting corrosion process. The aspect ratios of 1 and 3.5 wt. % NaCl are used to show how the pit diameters evolves during pitting corrosion process. 1 and 3.5% NaCl were chosen because pit diameter for 10 wt. NaCl was not recorded during measurements.

$$Aspect\ ratio\ = \frac{Dia_{max}}{d_{max}} \qquad \textbf{Equation 2}$$

When aspect ratio increases, it indicates that pit diameter increase at a higher rate than pit depth. When aspect ratio remains constant, either the pit diameter and pit depth are growing at proportional rate or both processes are being retarded at an equal rate. However, when aspect ratio decreases, it indicates that pit depth is increasing at a higher rate

than the pit diameter attack around the surrounding surface of an active pit.

It has already been shown that Fe_3C exposure results from Fe dissolution especially in the early stages of the corrosion process[1, 5, 26]. Therefore it is believed that the initial stages of pitting corrosion (pit initiation), is related to the role of revealed Fe_3C in establishing disntinct local anodic and cathodic sites (galvanic corrosion cells) across the corroding surface. It has previosly been shown that the overall progression of pitting corrosion is linked to the nature, morphology and protective capabilities of $FeCO_3$ formed over time[6]. $FeCO_3$ formed in this case is either an amorphous and/or polycrystalline (semi–protective) $FeCO_3$ corrosion product layer capable of supporting the progress of pitting corrosion[9, 31]. The initial Fe dissolution and establishment of Fe_3C is believed to be critical in the establishment of local anodic and cathodic sites. The protectiveness and/or semi-protectiveness of $FeCO_3$ is therefore hinged on the distribution of saturated species of Fe^{2+} and CO_3^{2-} at the corrosion interface for the formation of $FeCO_3$. The distribution of $FeCO_3$ across the corroding interface is likely to anchor preferentially on Fe_3C due to its lower overpotential for the cathodic reactions (HCO_3^-/CO_3^{2-}) than Fe[1, 32]. A combination of such Fe_3C-$FeCO_3$ distribution can lead to the establishment of galvanic effects between adjoining Fe-rich regions and Fe_3C-$FeCO_3$ rich regions, thereby accelerating the dissolution of Fe by accelerating the cathodic reaction adjacent to it.

By correlating the corrosion rate data in Figure 1, Figure 2, and Figure 3 for 30, 50 and 80°C, respectively with pitting corrosion data provided in Estimated thickness loss (µm) based on LPR measurements showing the synergistic effect of chloride ion concentration and temperature on carbon steel penetration after (a) 72 h and (b) 168 h. *Note: severity of material loss in magnitude increases in this order; Green → Amber → Red.*

Figure 11(a) and (b), Pitting corrosion in X65 carbon steel in different NaCl solutions over 168 h, at 30°C (a) Deepest pit, (b) average depth of pits and (c) Aspect ratio based on the diameter of deepest pit. *Note: Pit depth quantified after removal of corrosion product layer and Error bars on average depth of pits represents the standard deviation of 10 deepest pits*

Figure 12(a) and (b), and Pitting corrosion in X65 carbon steel in different NaCl solutions over 168 h, at 50°C (a) Deepest pit, (b) average depth of pits and (c) Aspect ratio based on the diameter of deepest pit. *Note: Pit depth quantified after removal of corrosion product layer and Error bars on average depth of pits represents the standard deviation of 10 deepest pits.*

Figure 13(a) and (b) for 30, 50 and 80°C, respectively, it is evident that the rate of Fe dissolution (and revealing of Fe_3C) and supersaturation at the corrosion interface is strongly linked with the evolution of pitting corrosion over 168 h. The depths of pits (average and deepest) after removal of corrosion products consistently show lowest values after 72 h for tests in 10 wt.% NaCl; ~13 µm at 30°C, ~22 µm at 50°C and ~24 µm at 80°C. These values were observed to be either lower than or equal to the pit depth for 1 wt. % NaCl; ~13 µm at 30°C, ~30 µm at 50°C and ~27 µm at 80°C. These observation shows that at high chloride concentration and higher temperature the depth of pits are lower due to higher rate of Fe dissolution which produces Fe^{2+} for the formation of $FeCO_3$. The pit depth is lower at lower chloride concentration and lower temperature due to the lower rate of Fe dissolution and hence lower rate of $FeCO_3$ formation. This is consistent with the previous discussion on how increasing chloride concentration and temperature increases the rate of saturation of corrosion interface for promoting the formation of $FeCO_3$. The implication of this effect is that with increasing exposure time, the rate of $FeCO_3$ formation increases as interfacial saturation increases, especially for high chloride and temperature systems. This also increases the protection from $FeCO_3$ covered areas, which are electrochemically distinct but connnected in a galvanic cell with locally corroding anodes, to support pit growth as shown by the increase in the depth of pits after 168 h in Estimated thickness loss (µm) based on LPR measurements showing the synergistic effect of chloride ion concentration and temperature on carbon steel penetration after (a) 72 h and (b) 168 h. *Note: severity of material loss in magnitude increases in this order; Green → Amber → Red.*

Figure 11(a) and(b), Pitting corrosion in X65 carbon steel in different NaCl solutions over 168 h, at 30°C (a) Deepest pit, (b) average depth of pits and (c) Aspect ratio based on the diameter of deepest pit. *Note: Pit depth quantified after removal of corrosion product layer and Error bars on average depth of pits represents the standard deviation of 10 deepest pits*

Figure 12(a) and (b), and Pitting corrosion in X65 carbon steel in different NaCl solutions over 168 h, at 50°C (a) Deepest pit, (b) average depth of pits and (c) Aspect ratio based on the diameter of deepest pit. *Note: Pit depth quantified after removal of corrosion product layer and Error bars on average depth of pits represents the standard deviation of 10 deepest pits.*

Figure 13(a) and (b) for 30, 50 and 80°C, respectively (10 wt.% NaCl; ~26 µm at 30°C, ~52 µm at 50°C and ~31 µm at 80°C compared to 1 wt.% NaCl; ~15 µm at 30°C, ~52 µm at 50°C and ~34 µm at 80°C). Between 72 h and 168 h and for test at 80°C the size of pit increased by ~30% for test in both 1 wt. % (from ~27 µm to ~34 µm) and 10 wt.% NaCl (from~24 µm to ~31 µm).

Although the final depth of pit is slightly higher in 1 wt.% NaCl, the results also shows that while increasing chloride concentration could increase the rate of $FeCO_3$ (although semi-protective) formation to support pit growth, its effect on Fe dissolution also supresses pitting corrosion contribution to total metal penetration. The reverse effect is observed with decreasing chloride concentration. For tests in 10 wt.% NaCl and between 72 and 168 h, pit depth only increased from ~13 µm to ~26 µm at 30°C, ~22 µm to ~52 µm at 50°C and ~24 µm to ~31 µm at 80°C, representing 50%, 136% and 30% increase for 30, 50 and 80°C respectively. At 30°C, low temperature supresses the aggressive effect of chloride ions needed to increase interfacial supersaturation and form semi-protective $FeCO_3$ that supports pit growth, especially as this temperature records the lowest general corrosion rate. At 80°C, the aggressiveness of chloride ions are enhanced to drive Fe dissolution (manifesting mainly as high general corrosion). This will lead to the formation of semi-protecive $FeCO_3$ capable of supporting significant pit growth. However, the size of pit is reduced by the receeding corroding interface due to general corrosion. At 50°C, the highest pit growth percentage increase was recorded because of the balancing effect of both Fe dissolution and $FeCO_3$ formation to support pit growth at this intermediate temperature. This is consistent with the general characterisation of $FeCO_3$ formed at temperatures ≤60°C as non-protective[1]; a precursor of pitting corrosion attack[9]. The results discussed in this section is considered a disntinctive corrosion characteristics of active metals such as carbon steel[7] and clearly shows that chloride concentration and temperature can act in synergy to determine the corrosion mechanism that dominates metal penetration

in CO_2 containing corrosion environments, especially when the corrosion environment is un-bufferred.

The aspect ratios for 1 and 3.5 wt.% NaCl are presented in Estimated thickness loss (µm) based on LPR measurements showing the synergistic effect of chloride ion concentration and temperature on carbon steel penetration after (a) 72 h and (b) 168 h. *Note: severity of material loss in magnitude increases in this order; Green → Amber → Red.*

Figure 11(c), Pitting corrosion in X65 carbon steel in different NaCl solutions over 168 h, at 30°C (a) Deepest pit, (b) average depth of pits and (c) Aspect ratio based on the diameter of deepest pit. *Note: Pit depth quantified after removal of corrosion product layer and Error bars on average depth of pits represents the standard deviation of 10 deepest pits*

Figure 12(c) and Pitting corrosion in X65 carbon steel in different NaCl solutions over 168 h, at 50°C (a) Deepest pit, (b) average depth of pits and (c) Aspect ratio based on the diameter of deepest pit. *Note: Pit depth quantified after removal of corrosion product layer and Error bars on average depth of pits represents the standard deviation of 10 deepest pits.*

Figure 13 (c) for 30, 50 and 80°C, respectively. Generally, an increase in aspect ratio implies that the diameter of pits is getting broader while the pit depth is becoming shallower. This is usually the case when there is significant contribution of general corrosion to metal penetration such that the surrounding surfaces around the pit is receding. When the aspect ratio is constant, it implies that either the rate at which the pit is growing depth-wise is equal to the rate at which the pit diameter is broadening by general corrosion or both processes are being retarded at an equal rate. When the aspect ratio is decreasing, it implies that the rate of pit growth is higher than the rate of diameter broadening due to general corrosion. On the premise of this, it is evident from Estimated thickness loss (µm) based on LPR measurements showing the synergistic effect of chloride ion concentration and temperature on carbon steel penetration after (a) 72 h and (b) 168 h. *Note: severity of material loss in magnitude increases in this order; Green → Amber → Red.*

Figure 11(c) that within the first 36 h, general corrosion dominated the material loss process in 3.5 wt. % NaCl than in 1 wt. % NaCl. This is shown by the higher aspect ratio. However, substantial pit growth is observed for 3.5 wt. % NaCl between 36-72 h after which the pit and diameter broadening rate remained almost the same. This coincides with the period of stable corrosion rate due to the establishment of semi-protective $FeCO_3$ on the corroding surface. For 1 wt. % NaCl, aspect ratio increased significantly with time until 120 h, showing a period where general corrosion dominates metal penetration. At 50°C, aspect ratio after 7 h show a substantial decrease (increase in pit depth compared to increase in pit diameter) in 1 wt. % NaCl while it remained constant 3.5 wt. % NaCl. This corroborates the increase in general corrosion contribution with increase in chloride concentration (3.5 wt. % NaCl) and high temperature to cause pit depth to be increasing at the same rate as the diameter is increasing. This can be described as the "broadening of pit". At 80°C, the aspect ratio decreases after 7 h (3.5 wt.%) and 36 h (1 wt.%) to indicate a period of higher pit growth rate than the rate of increase of diameter until after 72 h when the general corrosion rate becomes dominant. At this stage the diameter of pit increases faster than pit growth and the surface of pit will recede faster.

The results from this study, particularly the aspect ratio shows the effect of highly dynamic and complex interfacial phenomena that supports pitting corrosion process. General corrosion is able to impose limitations on pitting corrosion behavior of carbon steel to such an extent that the pit growth rate become seemingly retarded depending on the conditions. Pit retardation can also be due to localized self-healing of pits due to local saturation with precipitable anions [6, 12]. Chloride ion concentration and temperature have been shown in this study to have strong effect in how all of these interfacial phenomena act in synergy to determine the relative dominance of a suit of corrosion mechanisms driving metal penetration.

The results discussed above also explains the complex means by which chloride ions influences the pitting corrosion characteristics of carbon steel materials in un-buffered CO_2 corrosion environments. They are consistent with the evolution of pitting corrosion from a starting point of Fe dissolution (and Fe_3C revelation) and $FeCO_3$ formation. Therefore, in conditions where $FeCO_3$ has not been pre-formed as is the case in this study, the effect of chloride concentration on the general and pitting corrosion characteristics is therefore correlated on the corrosivity of the environment and how it translates into the different processes that leads to pitting corrosion; Fe dissolution and formation of non-protective $FeCO_3$. This is consistent with the understanding that if $FeCO_3$ does not form, metal corrosion will be completely dominated by general corrosion[9] and if a completely protective and non-porous $FeCO_3$ layer forms without any local galvanic cell and/or local anode, pitting corrosion is almost absent. Thus, any corrosion scenario that falls in between these absolutes will lead to a certain degree of pitting corrosion. However, once a protective $FeCO_3$ is formed, the mechanism of influence of chloride ion may change to become more of a destructive agent to the integrity of protective $FeCO_3$[2].

Figure 14(a) and (b), presents evidence of the relationship between the synergy of chloride ion concentration and temperature on total metal penetration after 72 h and 168 h. This is also presented in terms of the relationship between pitting factor and the synergistic effect of chloride ion and temperature in Matrix to qualify the effect of synergy of chloride ion concentration and temperature on total metal penetration of carbon steel after (a) 72 h and (b) 168 h. *Note: severity of material loss in magnitude increases in this order; Green → Amber → Red.*

Figure 15(a) and (b). The concept of pitting factor (P_f) has been introduced in previous publications [6, 11] and used to reflect the relative contribution of corrosion damage mechanisms; general and pitting corrosion to metal penetration. It is defined in ASTM standard G46-94[21] as:

Pitting Factor; $$P_f = \left(\frac{P_d}{P_u}\right)$$ **Equation 3**

Where P_d is the deepest metal penetration (µm) for the whole exposed surface area (sum of depth of deepest pit (d_{max}), (after removal of corrosion products) plus the average estimated metal penetration (µm) from general corrosion rate measurement (termed P_u), i.e; $P_d = P_u + d_{max}$. A pitting factor of 1 represents general corrosion; i.e., $P_d = P_u$, and $d_{max} = 0$. The greater the (d_{max}), the greater the pitting factor.

Referring to Matrix to qualify the effect of synergy of chloride ion concentration and temperature on total metal penetration of carbon steel after (a) 72 h and (b) 168 h. *Note: severity of material loss in magnitude increases in this order; Green → Amber → Red.*

Figure 15 and according to ASTM standard G46-94[21], a higher pitting factor indicates a lower contribution to metal penetration from general corrosion. The "threshold effect" can be observed in the pitting factor data at 30˚C and slowly disappears with increasing temperature at higher temperature within the first 36 h (Matrix to qualify the effect of synergy of chloride ion concentration and temperature on total metal penetration of carbon steel after (a) 72 h and (b) 168 h. *Note: severity of material loss in magnitude increases in this order; Green → Amber → Red.*

Figure 15(a)), while the effect of general corrosion is evident in the lower pitting factor after 72 and 168 h for all conditions (Matrix to qualify the effect of synergy of chloride ion concentration and temperature on total metal penetration of carbon steel after (a) 72 h and (b) 168 h. *Note: severity of material loss in magnitude increases in this order; Green → Amber → Red.*

Figure 15(b) and (c)). At the higher temperature of 80°C, the results on pitting factor shown in Matrix to qualify the effect of synergy of chloride ion concentration and temperature on total metal penetration of carbon steel after (a) 72 h and (b) 168 h. *Note: severity of material loss in magnitude increases in this order; Green → Amber → Red.*

Figure 15 suggests that the pitting characteristics of carbon steel is limited by the extent of general corrosion and $FeCO_3$ formation. While the actual ionic/electrochemical interaction of Cl^- within an active pit on carbon steel still remain unclear and could not be established in this study, it is clear that such interaction will be different from the auto catalytic changes in local chemistry and pit propagation in stainless steel in the presence of Cl^-. Therefore, it is believed that the increase in the total metal penetration with increase in chloride ion concentration and temperature as shown in Figure 14 is related to the process of thermal activation.

Conclusions

The effect and synergy of chloride concentration and temperature on carbon steel corrosion behavior; general and pitting corrosion in CO_2 containing corrosion environment have been investigated over 168 h. The key conclusions from this work are presented herein:

- Chloride ion concentration and temperature can independently and synergistically influence the overall corrosion characteristic; general and pitting corrosion of carbon steel to determine the extent of metal penetration. This is correlated on their influence on the rate of ferrite dissolution, and $FeCO_3$ formation kinetics and properties.

- Generally, the rate of general corrosion increases with temperature and chloride concentration. However, at lower temperatures, the effect of chloride ion concentration is strongly linked to the "*salting out effect*" on CO_2 gas solubility and aggressiveness of the environment. The competition of these phenomena activates the emergence of the *"threshold effect"* on the influence of chloride ion concentration on corrosion rate at lower temperatures, particularly in the early stages of the corrosion process.

- At higher temperature, the *"Arrhenius effect"* of temperature causes the thermal activation of Cl^- species to increase the aggressiveness of the corrosion environment and driving the Fe dissolution process for $FeCO_3$ formation. The synergy of thermal activation of chloride species increases rate of metal corrosion; including general and pitting corrosion. This synergy, especially with increasing chloride concentration and temperature, promotes the transition from amorphous and/or polycrystalline $FeCO_3$ to crystalline $FeCO_3$ due to increased saturation of corrosion interface with ferrous ions.

- The extent of metal penetration from pitting corrosion is also observed to be related to the ability of chloride ions and temperature effect to act synergistically to promote the formation of semi-protective $FeCO_3$. The rate of formation of this type of $FeCO_3$ increases with increasing chloride concentration, especially with increasing temperature from 30 to 50˚C and supporting higher pit penetration depth.

- Based on pitting factor analysis, the "threshold effect" of chloride ions is also evident in the pitting initiation process; remaining still dominant at 30˚C. At higher temperatures (80˚C) and higher chloride concentration (10 wt. % NaCl), the threshold effect is replaced by the masking effect of pit penetration depth by the higher contribution from general corrosion to highlight the impact of the synergy of chloride and temperature on total metal penetration.

References

1. B.M. Kermani and A. Morshed, "Carbon dioxide corrosion in oil and gas production: A compendium", Corrosion, 59, 08 (2003): p. 659-683.

2. X. Gao, B. Brown, and S. Nesic. "Effect of chloride on localized corrosion initiation of carbon steel in a CO_2 aqueous environment", CORROSION, paper no. 3880, (San Antonio, TX: NACE International, 2014).

3. Q.Y. Liu, L.J. Mao, and S.W. Zhou, "Effects of chloride content on CO_2 corrosion of carbon steel in simulated oil and gas well environments", Corrosion Science, 84, 0 (2014): p. 165-171.

4. M.B. Kermani and D. Harrop, "The impact of corrosion on oil and gas industry", SPE Production & Operations, 11, 3 (1996): p. 186-190.

5. J.L. Crolet, N. Thevenot, and S. Nesic, "Role of Conductive Corrosion Products in the Protectiveness of Corrosion Layers", Corrosion, 54, 3 (1998): p. 194-203.

6. F. Pessu, R. Barker, and A. Neville, "Understanding Pitting Corrosion Behavior of X65 Carbon Steel in CO_2-Saturated Environments: The Temperature Effect", Corrosion, 72, 1 (2015): p. 78-94.

7. R.E. Melchers, "Pitting corrosion of mild steel in marine immersion environment—Part 1; Maximum pit depth", Corrosion, 60, 9 (2004): p. 824-836.

8. X. Lou and P.M. Singh, "Role of water, acetic acid and chloride on corrosion and pitting behaviour of carbon steel in fuel-grade ethanol", Corrosion Science, 52, 7 (2010): p. 2303-2315.

9. S. Papavinasam, A. Doiron, and R.W. Revie, "Model to predict internal pitting corrosion of oil and gas pipelines", Corrosion, 66, 3 (2010): p. 11.

10. S. Papavinasam, A. Doiron, J. Li, D.-Y. Park, and P. Liu. "Sour and sweet corrosion of carbon steel: general or pitting or localized or all of the above?", CORROSION, paper no. 332, (San Antonio, TX: NACE International, 2010).

11. F. Pessu, R. Barker, and A. Neville, "The Influence of pH on Localized Corrosion Behavior of X65 Carbon Steel in CO_2 Saturated Brines", Corrosion, 71, 12 (2015): p. 1452-1466.

12. G. Schmitt and S. Feinen. "Effect of anions and cations on the pit initiation in CO_2 corrosion of iron and steel", CORROSION, paper no.01, (Orlando, FL: NACE International, 2000).

13. F.F. Eliyan, F. Mohammadi, and A. Alfantazi, "An electrochemical investigation on the effect of the chloride content on CO_2 corrosion of API-X100 steel", Corrosion Science, 64, 0 (2012): p. 37-43.

14. S. Nešić, "Key issues related to modelling of internal corrosion of oil and gas pipelines – A review", Corrosion Science, 49, 12 (2007): p. 4308-4338.

15. N. Anselmo, J.E. May, N.A. Mariano, P.A.P. Nascente, and S.E. Kuri, "Corrosion behavior of supermartensitic stainless steel in aerated and CO_2-saturated synthetic seawater", Materials Science and Engineering: A, 428, 1–2 (2006): p. 73-79.

16. K.-M. Yap and S. Srinivasan. "Key factors in development of a CO_2-H_2S corrosion prediction model for multiphase oil-gas production systems", CORROSION, 374, (Houston, TX: NACE International, 2010).

17. A.S.M. International, *Metals Handbook, Ninth Edition: Volume 13-Corrosion (ASM Handbook)*, 1987, ASM International Ohio p. 236-241.

18. X. Jiang, S. Nešić, B. Kinsella, B. Brown, and D. Young, "Electrochemical investigation of the role of Cl^- on localized carbon dioxide corrosion behavior of mild steel", Corrosion, 69, 1 (2012): p. 15-24.

19. H. Fang, B. Brown, and S. Nešić, "Effects of sodium chloride concentration on mild steel corrosion in slightly sour environments", Corrosion, 67, 1 (2011): p. 015001-1-015001-12.

20. T. das Chagas Almeida, M.C.E. Bandeira, R.M. Moreira, and O.R. Mattos, "New insights on the role of CO_2 in the mechanism of carbon steel corrosion", Corrosion Science, 120, (2017): p. 239-250.

21. A.S.T.M. International, *ASTM G46-94 Standard Guide for Examination and Evaluation of Pitting Corrosion*, 2005, ASTM International: West Conshohocken, PA. p. 7.

22. H. Fang, B. Brown, and S. Nesić. "High salt concentration effects on CO_2 corrosion and H2S corrosion", CORROSION paper no. 276, (San Antonio, TX: NACE International, 2010).

23. Q.Y. Liu, L.J. Mao, and S.W. Zhou, "Effects of chloride content on CO_2 corrosion of carbon steel in simulated oil and gas well environments", Corrosion Science, 84, (2014): p. 165-171.

24. F.F. Eliyan and A. Alfantazi, "Influence of temperature on the corrosion behavior of API-X100 pipeline steel in 1-bar CO_2-HCO_3^- solutions: An electrochemical study", Materials Chemistry and Physics, 140, 2–3 (2013): p. 508-515.

25. S. Guo, L. Xu, L. Zhang, W. Chang, and M. Lu, "Corrosion of alloy steels containing 2% chromium in CO_2 environments", Corrosion Science, 63, (2012): p. 246-258.

26. J. Han, B.N. Brown, and S. Nešić, "Investigation of the galvanic mechanism for localized carbon dioxide corrosion propagation using the artificial pit technique", Corrosion, 66, 9 (2010): p. 12.

27. H. Hoffmeister. "Modelling the effect of chloride content on H_2S corrosion by coupling of phase and polarization behavior", COROSION, paper no. 501, (Nashville, TN: NACE International, 2007).

28. Y. Zheng, B. Brown, and S. Nešić, "Electrochemical study and modelling of H_2S corrosion of mild steel", Corrosion, 70, 4 (2013): p. 351-365.

29. S. Nesic, J. Postlethwaite, and S. Olsen, "An electrochemical model for prediction of corrosion of mild steel in aqueous carbon dioxide solutions", Corrosion, 52, 04 (1996): p. 280-294.

30. W. Sun, S. Nešić, and R.C. Woollam, "The effect of temperature and ionic strength on iron carbonate ($FeCO_3$) solubility limit", Corrosion Science, 51, 6 (2009): p. 1273-1276.

31. Z. Xia, K.C. Chou, and Z. Szklarska-Smialowska, "Pitting corrosion of carbon steel in CO_2-containing NaCl brine", Corrosion, 45, 8 (1989): p. 636-642.

32. J. Crolet, N. Thevenot, and S. Nesic, "Role of Conductive Corrosion Products in the Protectiveness of Corrosion Layers", Corrosion, 54, 3 (1998): p. 194-203.

33. I.G. Wood, L. Vocadlo, K.S. Knight, D.P. Dobson, W.G. Marshall, and G.D.B. Price, J., "Thermal expansion and crystal structure of cementite, Fe3C, between 4 and 600 K determined by time-of-flight neutron powder diffraction Note:T=540 K", Journal of Applied Crystallography, 37, (2004): p. 9.

34. K.M. H. Effenberger, and J. Zemann, "Crystal structure refinements of magnesite, calcite, rhodochrosite, siderite, smithonite, and dolomite, with discussion of some aspects of the stereochemistry of calcite type carbonates", Z. Kristallogr, 156, (1981): p. 11.

35. F. Deganello, L.F. Liotta, A. Longo, M.P. Casaletto, and M. Scopelliti, "Cerium effect on the phase structure, phase stability and redox properties of Ce-doped strontium ferrates", Journal of Solid State Chemistry, 179, 11 (2006): p. 3406-3419.

36. M. Abe, M. Kawachi, and S. Nomura, "X-Ray and Neutron Diffraction Studies in Spinel Fe_2MoO_4", Journal of the Physical Society of Japan, 33, 5 (1972): p. 1296-1302.

37. D.-Q. Zheng, T.-M. Guo, and H. Knapp, "Experimental and modeling studies on the solubility of CO_2, $CHClF_2$, CHF_3, $C_2H_2F_4$ and $C_2H_4F_2$ in water and aqueous NaCl solutions under low pressures", Fluid Phase Equilibria, 129, 1–2 (1997): p. 197-209.

FIGURE CAPTIONS

Figure 1: Plots of (a) corrosion rate and (b) in-situ bulk pH for corrosion system of X65 carbon steel in 1, 3.5 and 10 wt. % NaCl soln. saturated with CO_2 at 30°C.

Figure 2: Plots of (a) corrosion rate and (b) in-situ bulk pH for corrosion system of X65 carbon steel in 1, 3.5 and 10 wt. % NaCl soln. saturated with CO_2 at 50°C.

Figure 3: Plots of (a) corrosion rate and (b) in-situ bulk pH for corrosion system of X65 carbon steel in 1, 3.5 and 10 wt. % NaCl soln. saturated with CO_2 at 80°C.

Figure 4: SEM of corrosion products formed on X65 carbon steel at 30°C after 168 h in (a) 1 wt. % NaCl soln., (b) 3.5 wt. % NaCl soln., and (c) 10 wt. % NaCl soln.

Figure 5: XRD patterns for (a) 1 wt. % and (b) 10 wt. % NaCl soln. for 168 h at 30°C (Note that the intensity scale is arbitrary). XRD patterns are referenced to the literature [33-36].

Figure 6: SEM of corrosion products formed on X65 carbon steel at 50°C in (a) 1 wt. % NaCl soln., 7 h, (b) 1 wt. % NaCl soln., 168 h (c) 3.5 wt. % NaCl soln., 7 h (d) 3.5 wt. % NaCl soln., 168 h, (e) 10wt. % NaCl soln., 7 h, and (f) 10 wt. % NaCl soln., 168 h.

Figure 7: XRD patterns for (a) 1 wt. % and (b) 10 wt. % NaCl soln. for 168 h at 50°C (Note that the intensity scale is arbitrary). XRD patterns are referenced to the literature [33-36].

Figure 8: SEM of corrosion products formed on X65 carbon steel at 80°C in (a) 1 wt. % NaCl soln., 7 h, (b) 1 wt. % NaCl soln., 168 h (c) 3.5 wt. % NaCl soln., 7 h (d) 3.5 wt. % NaCl soln., 168 h, (e) 10wt. % NaCl soln., 7 h, and (f) 10 wt. % NaCl soln., 168 h.

Figure 9: XRD patterns for (a) 1 wt. % and (b) 10 wt. % NaCl soln. for 168 h at 80°C (Note that the intensity scale is arbitrary). XRD patterns are referenced to the literature [33-36].

Figure 10: Estimated thickness loss (μm) based on LPR measurements showing the synergistic effect of chloride ion concentration and temperature on carbon steel penetration after (a) 72 h and (b) 168 h. *Note: severity of material loss in magnitude increases in this order; Green → Amber → Red.*

Figure 11: Pitting corrosion in X65 carbon steel in different NaCl solutions over 168 h, at 30°C (a) Deepest pit, (b) average depth of pits and (c) Aspect ratio based on the diameter of deepest pit. *Note: Pit depth quantified after removal of corrosion product layer and Error bars on average depth of pits represents the standard deviation of 10 deepest pits*

Figure 12 : Pitting corrosion in X65 carbon steel in different NaCl solutions over 168 h, at 50°C (a) Deepest pit, (b) average depth of pits and (c) Aspect ratio based on the diameter of deepest pit. *Note: Pit depth quantified after removal of corrosion product layer and Error bars on average depth of pits represents the standard deviation of 10 deepest pits.*

Figure 13 Pitting corrosion in X65 carbon steel in different NaCl Soln. over 168 h, at 80°C (a) size of deepest pit and (b) average size of pit. *Note: Pit depth quantified after removal of corrosion product layer and Error bars on average depth of pits represents the standard deviation of 10 deepest pits.*

Figure 14: Matrix to qualify the effect of synergy of chloride ion concentration and temperature on total metal penetration of carbon steel after (a) 72 h and (b) 168 h. *Note: severity of material loss in magnitude increases in this order; Green → Amber → Red.*

Figure 15: Matrix to qualify the effect of synergy of chloride ion concentration and temperature on the contribution to metal penetration from both pitting and generalgeneral corrosion in terms of pitting factor on carbon steel after (a) 36 h, (b) 72 h and (c) 168 h. *Note: severity of material loss in magnitude increases in this order; Green → Amber → Red.*

TABLES

Table 1: Temperature and total partial pressures of CO_2 gas at atmospheric pressure above test solution

Temperature (°C)	CO_2 partial pressure (kPa)
30	97
50	89
80	55

Table 2: X65 carbon steel composition (wt. %)

C	Si	P	S	Mo	Mn	Ni	Nb	V	Fe
0.15	0.22	0.023	0.002	0.17	1.42	0.09	0.05	0.06	97.81

Table 3: Dissolved CO_2 at experimental for assessing the effect of temperature and chloride conc. on corrosion of carbon steel.

NaCl Conc. (Wt. %)	Temperature (°C)		
	Dissolved CO_2 (ppm)		
	30°C	50°C	80°C
1	1242	763	458
3.5	977	595	382
10	594	297	158

Solubility data for dissolved CO_2 (Table 3) is calculated using experimentally determined Henry's coefficients for CO_2 in water at different NaCl solutions and at different temperatures by Zheng et al.[37].

Table 4: Tafel constants for each experimental conditions investigated for the effect of temperature and chloride conc.

T(˚C)	Tafel Parameters (mV/dec)								
	1 wt.% NaCl			3.5 wt.% NaCl			10 wt.% NaCl		
	β_a	β_c	B	β_a	β_c	B	β_a	β_c	B
80	47	85	13	58	135	18	75	140	21

50	40	120	13	40	168	14	55	160	18
30	35	145	12	33	200	12	43	180	15

1

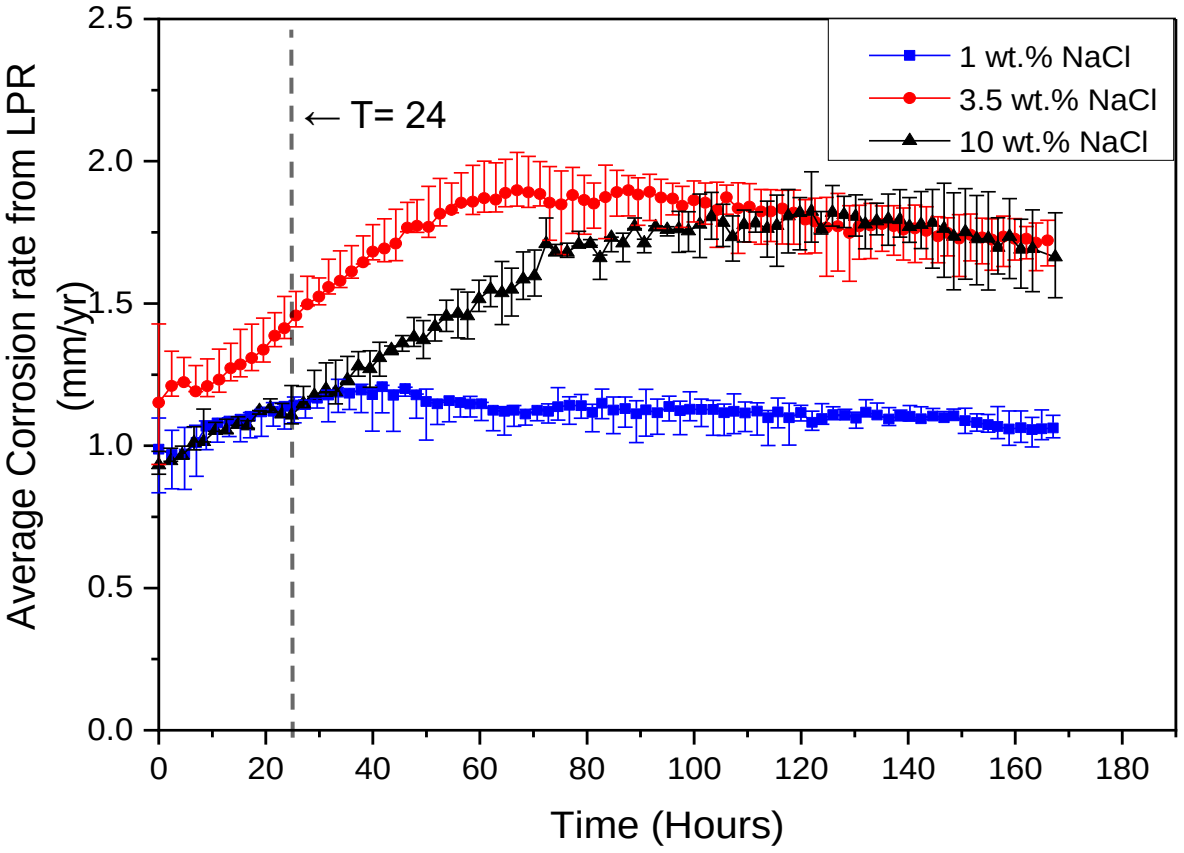

(a)

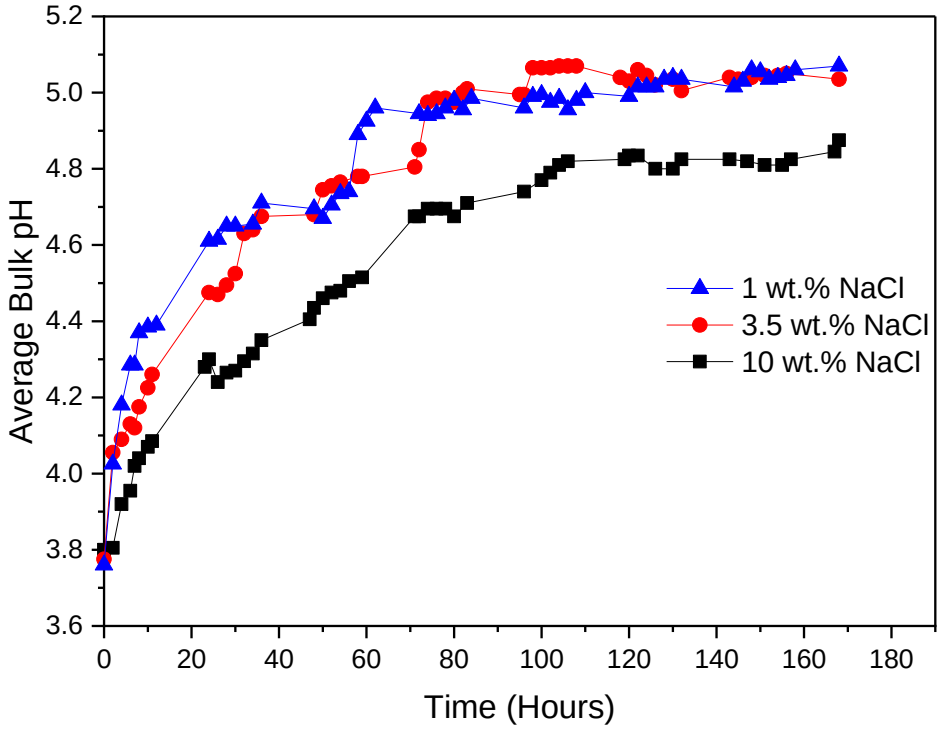

(b)

Figure 16: Plots of (a) corrosion rate and (b) in-situ bulk pH for corrosion system of X65 carbon steel in 1, 3.5 and 10 wt. % NaCl solutions saturated with CO_2 at 30°C.

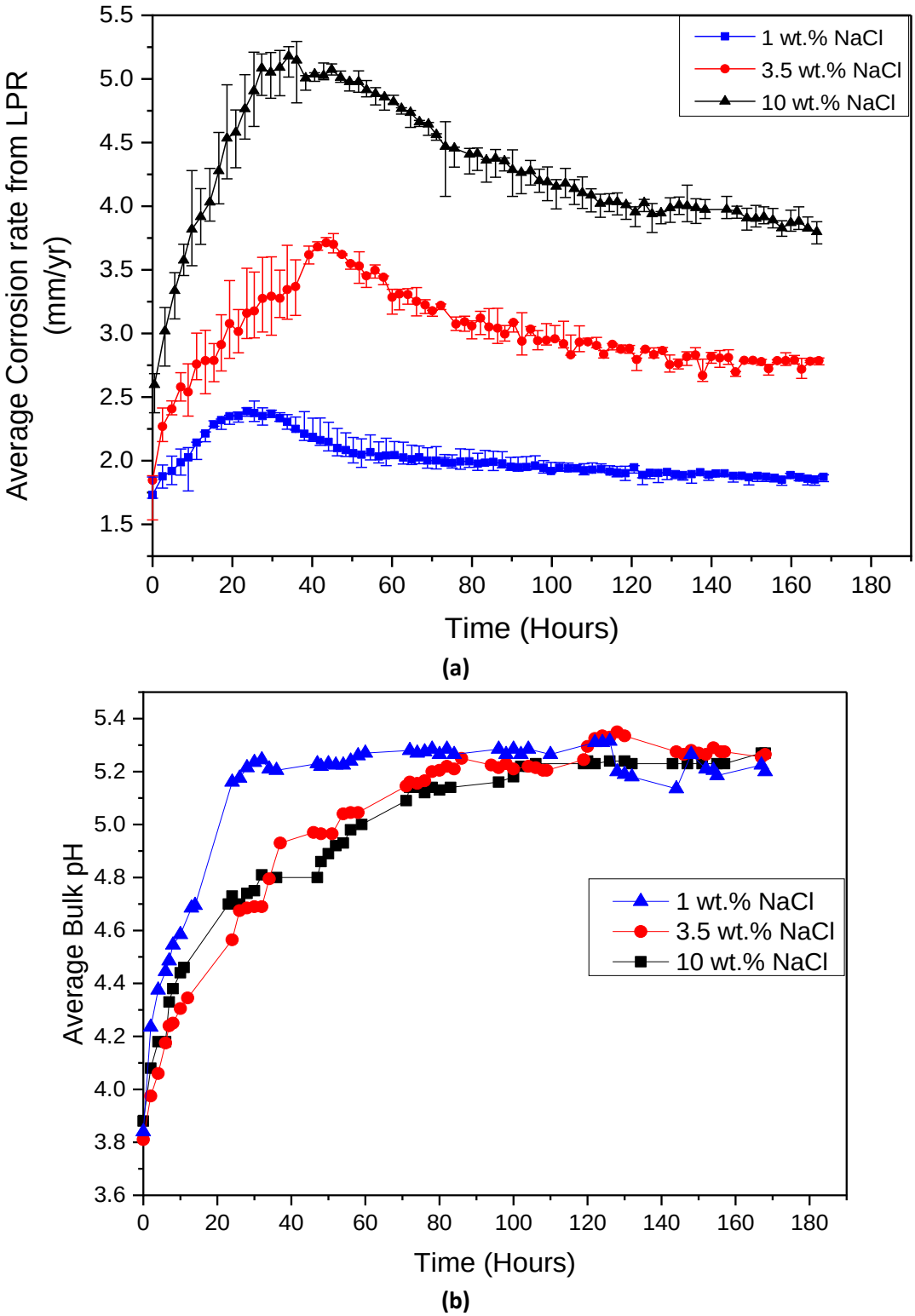

Figure 17: Plots of (a) corrosion rate and (b) in-situ bulk pH for corrosion system of X65 carbon steel in 1, 3.5 and 10 wt. % NaCl solutions saturated with CO_2 at 50°C.

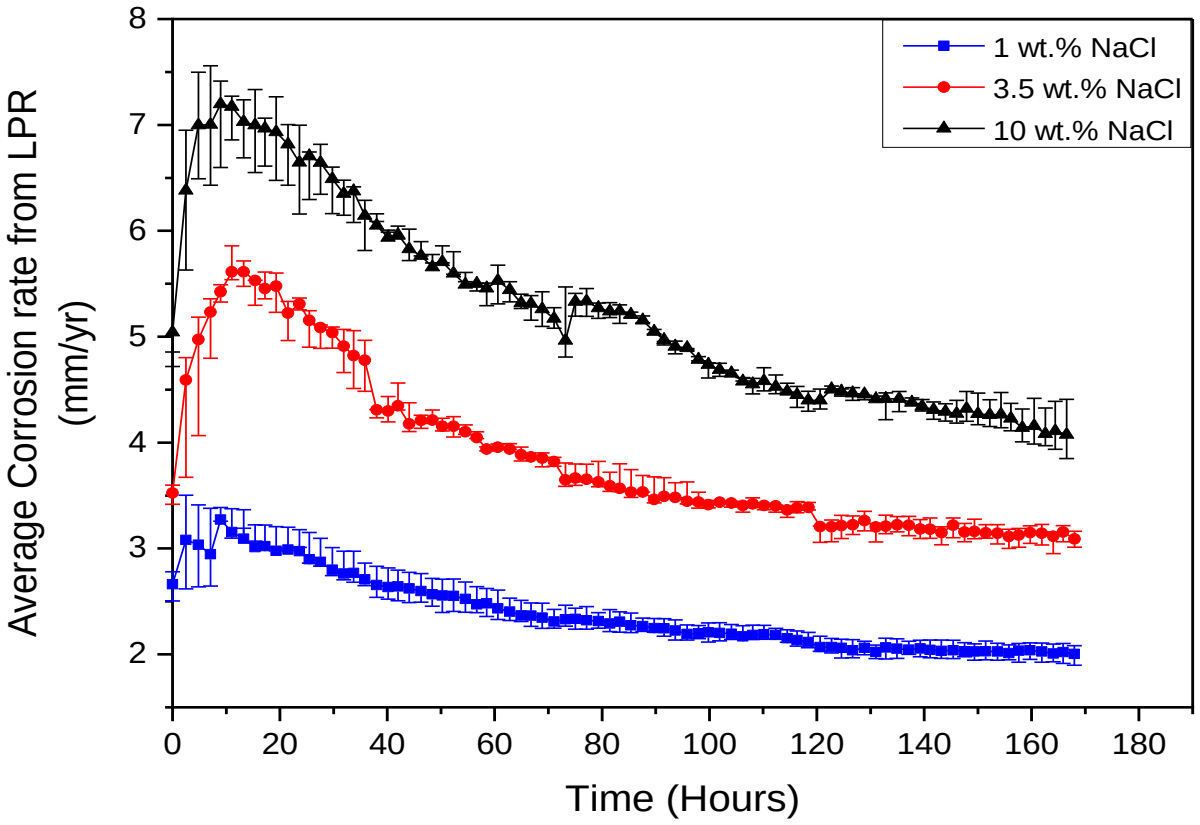

(a)

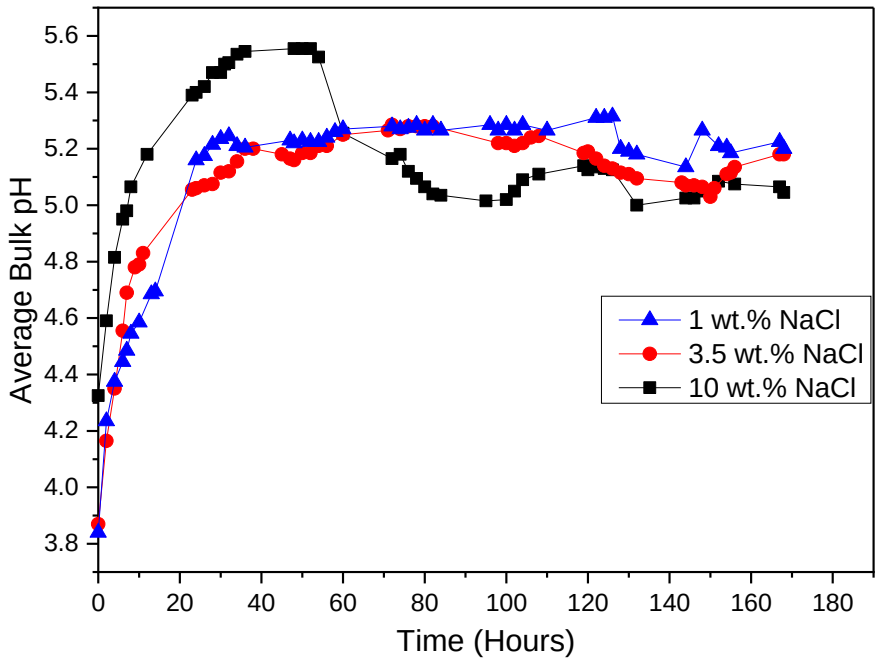

(b)

Figure 18: Plots of (a) corrosion rate and (b) in-situ bulk pH for corrosion system of X65 carbon steel in 1, 3.5 and 10 wt. % NaCl solutions saturated with CO_2 at 80°C.

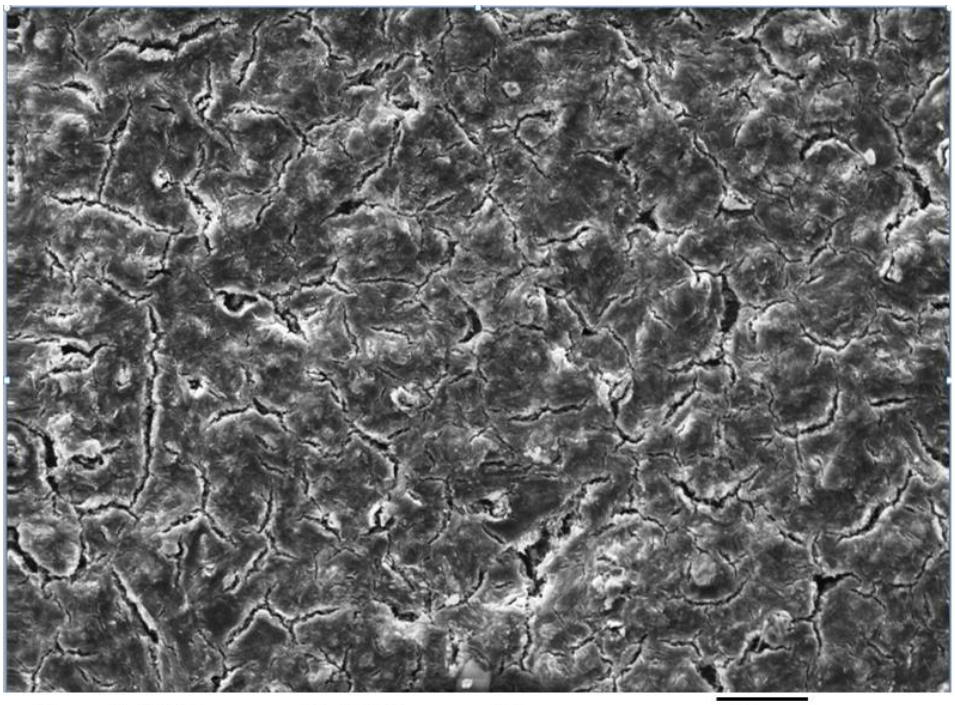

(a)

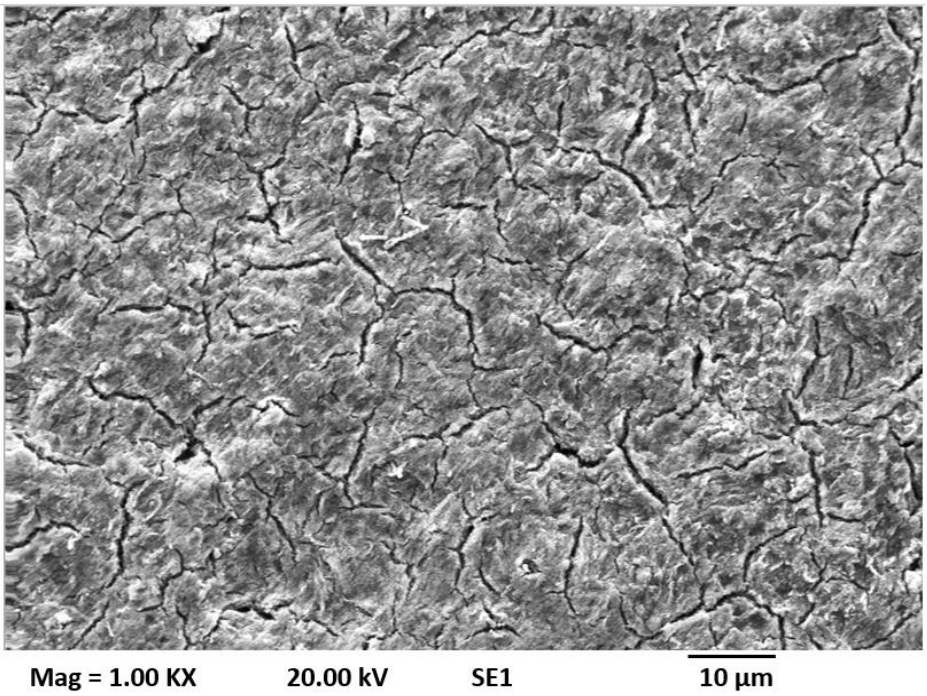

(b)

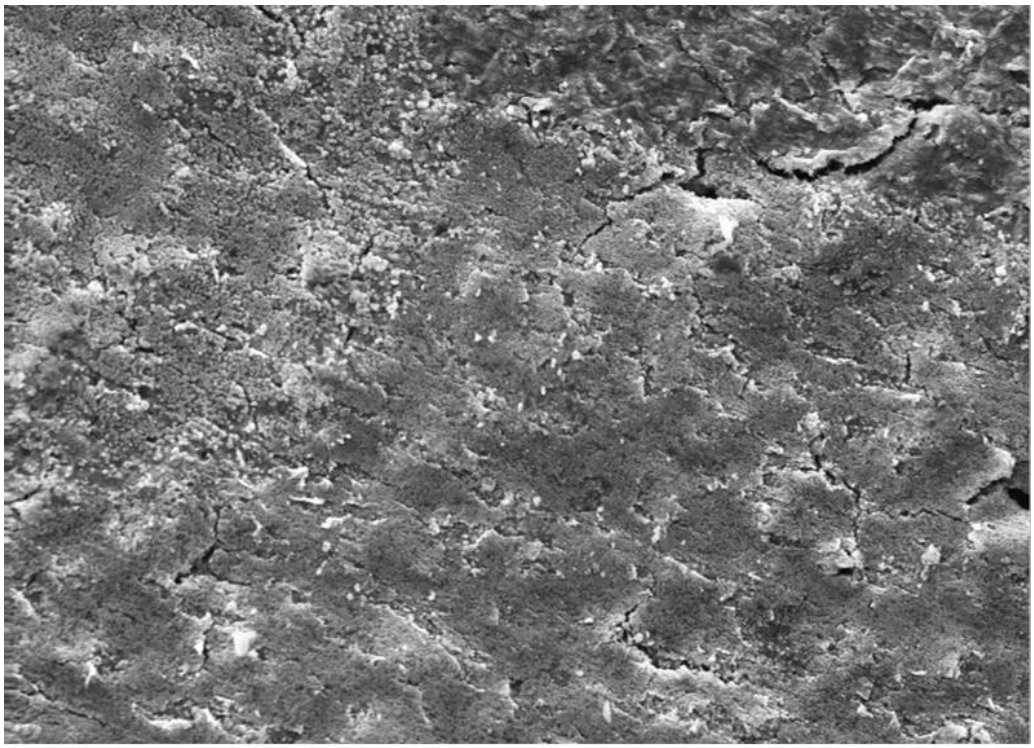

(c)

Figure 19: SEM of corrosion products formed on X65 carbon steel at 30°C after 168 h in (a) 1 wt. % NaCl, (b) 3.5 wt. % NaCl, and (c) 10 wt. % NaCl solutions.

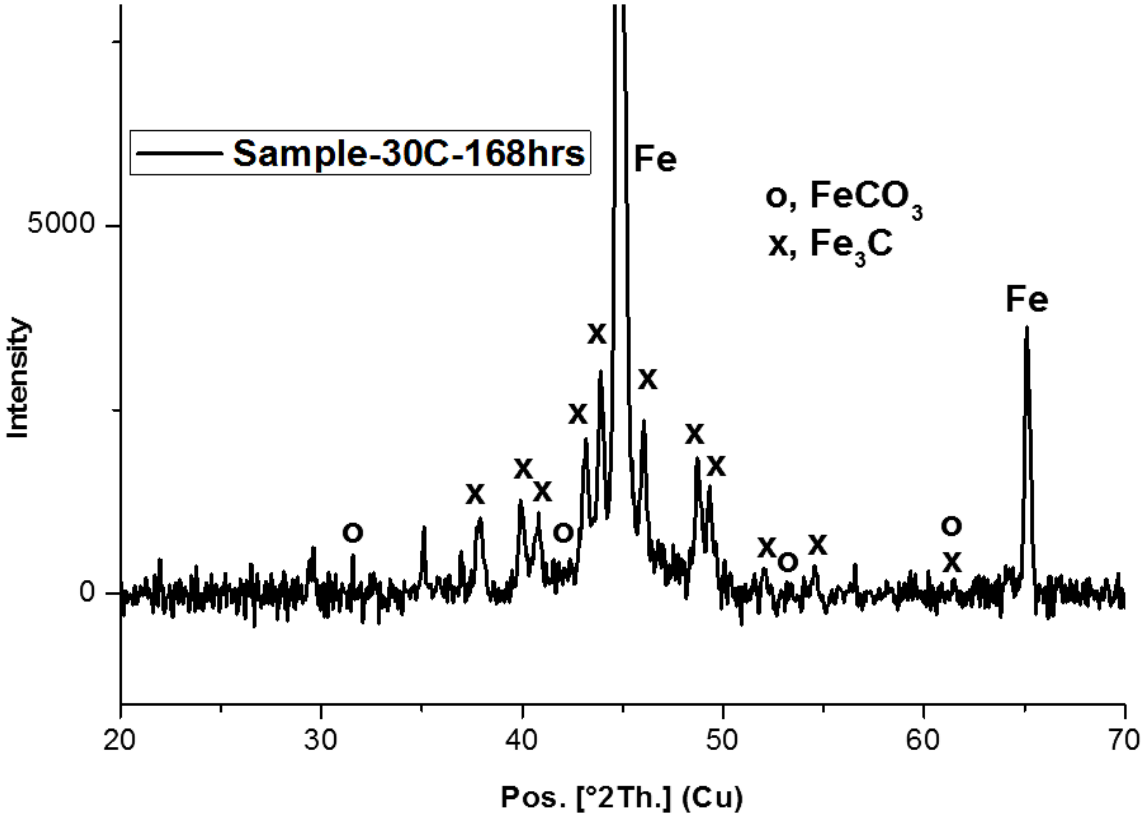

(a)

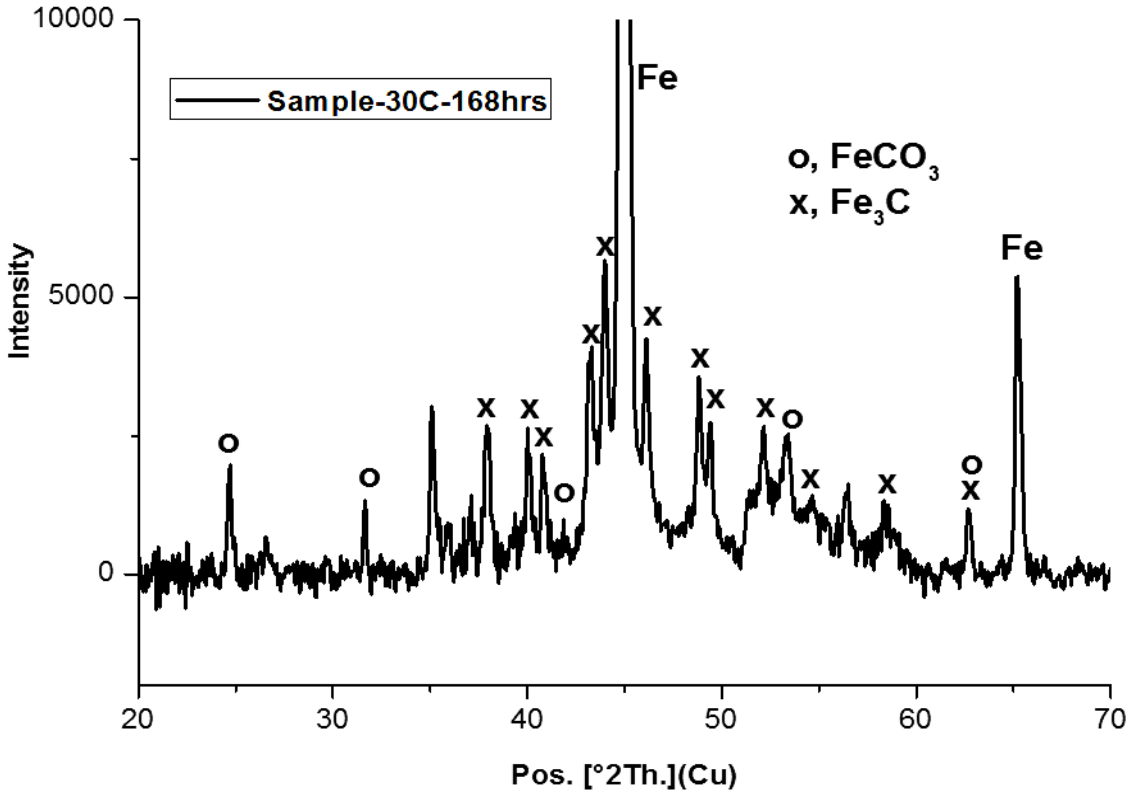

(b)

Figure 20: XRD patterns for (a) 1 wt. % and (b) 10 wt. % NaCl solutions for 168 h at 30°C (Note that the intensity scale is arbitrary). XRD patterns are referenced to the literature [33-36].

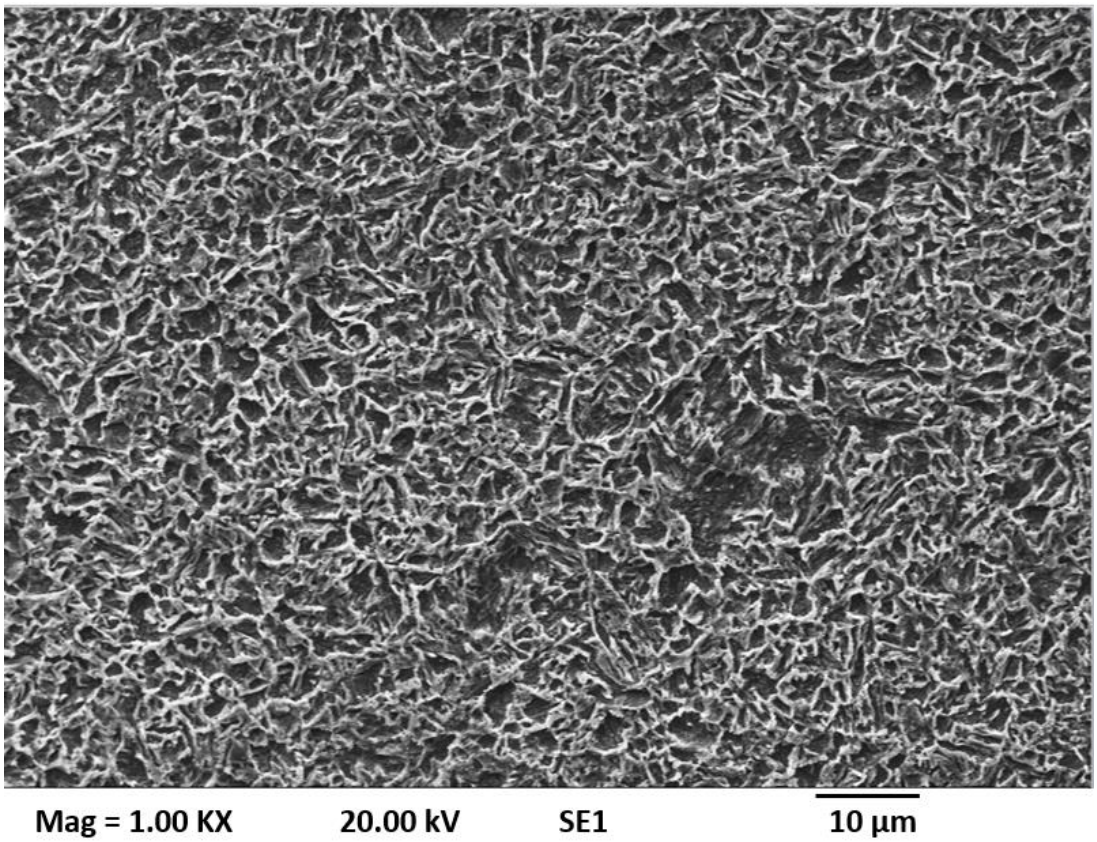

(a)

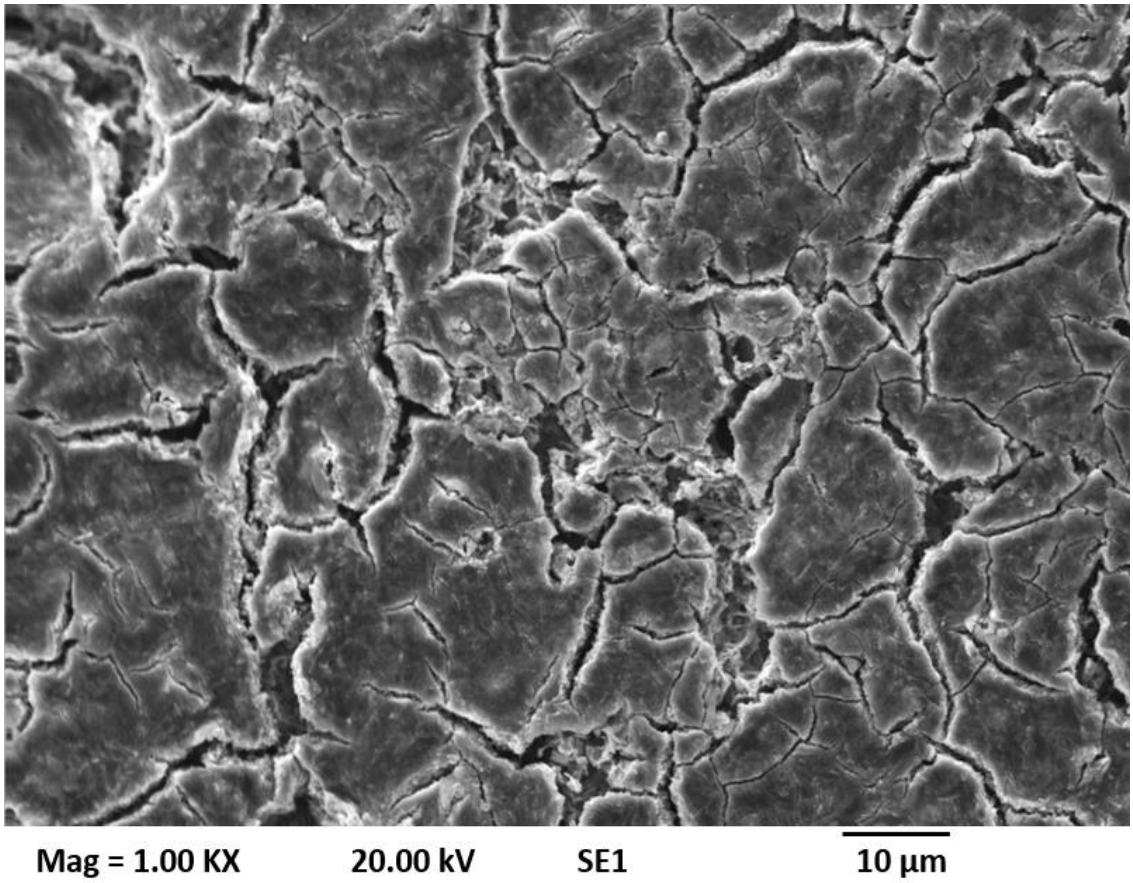

(b)

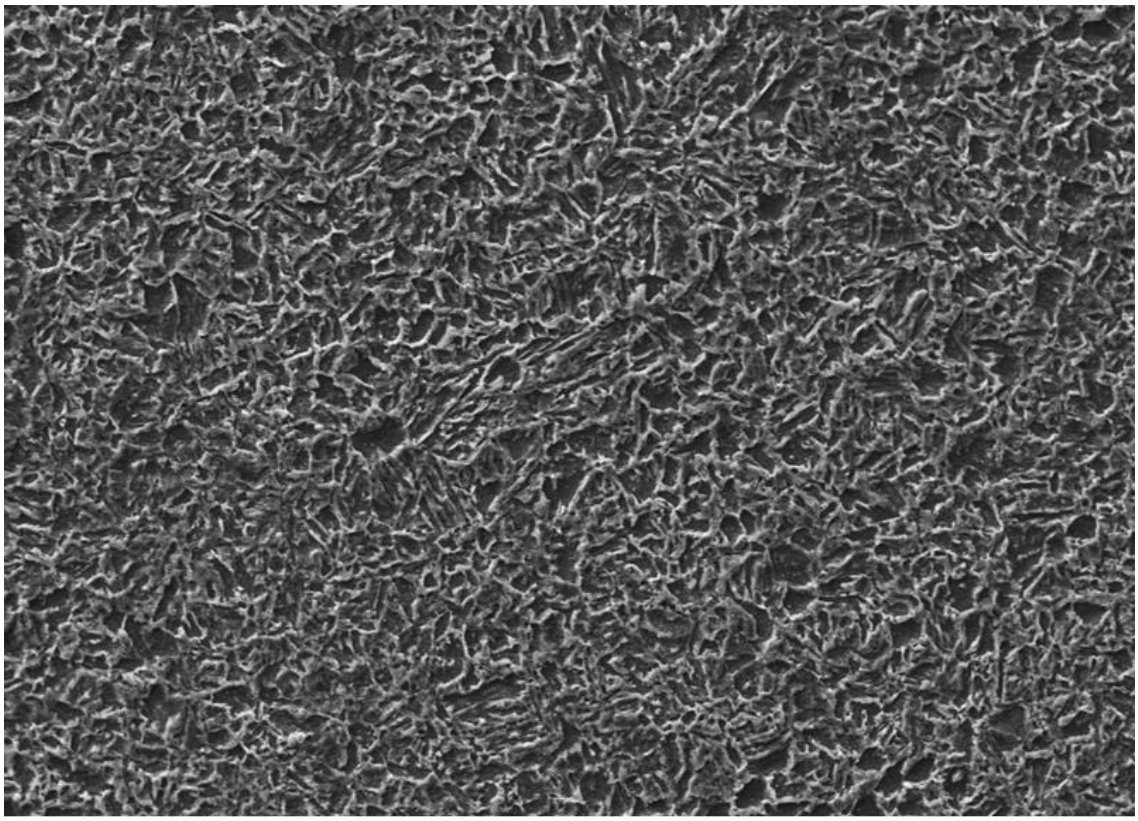

(c)

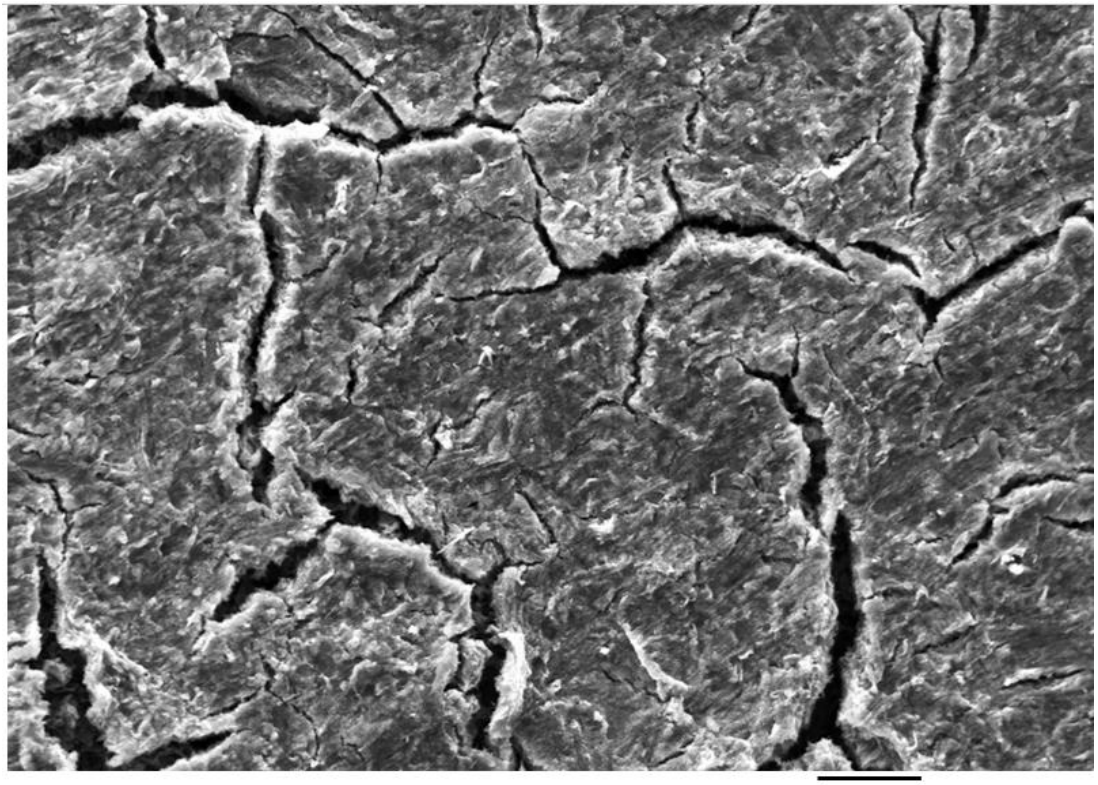

(d)

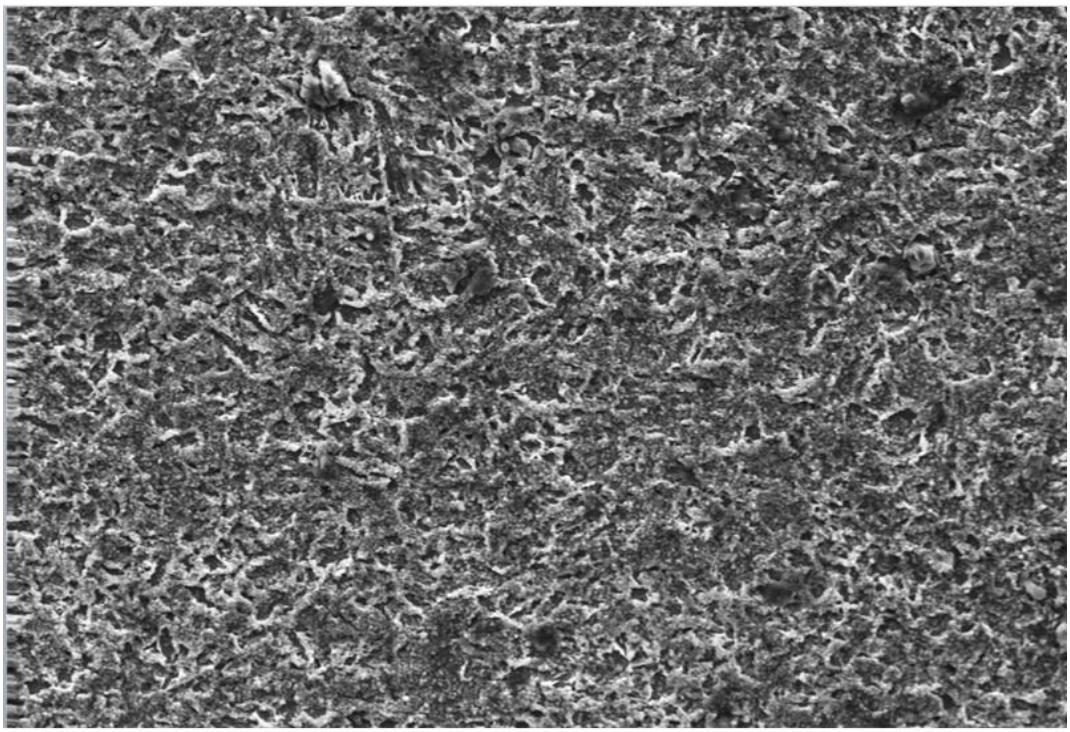

(e)

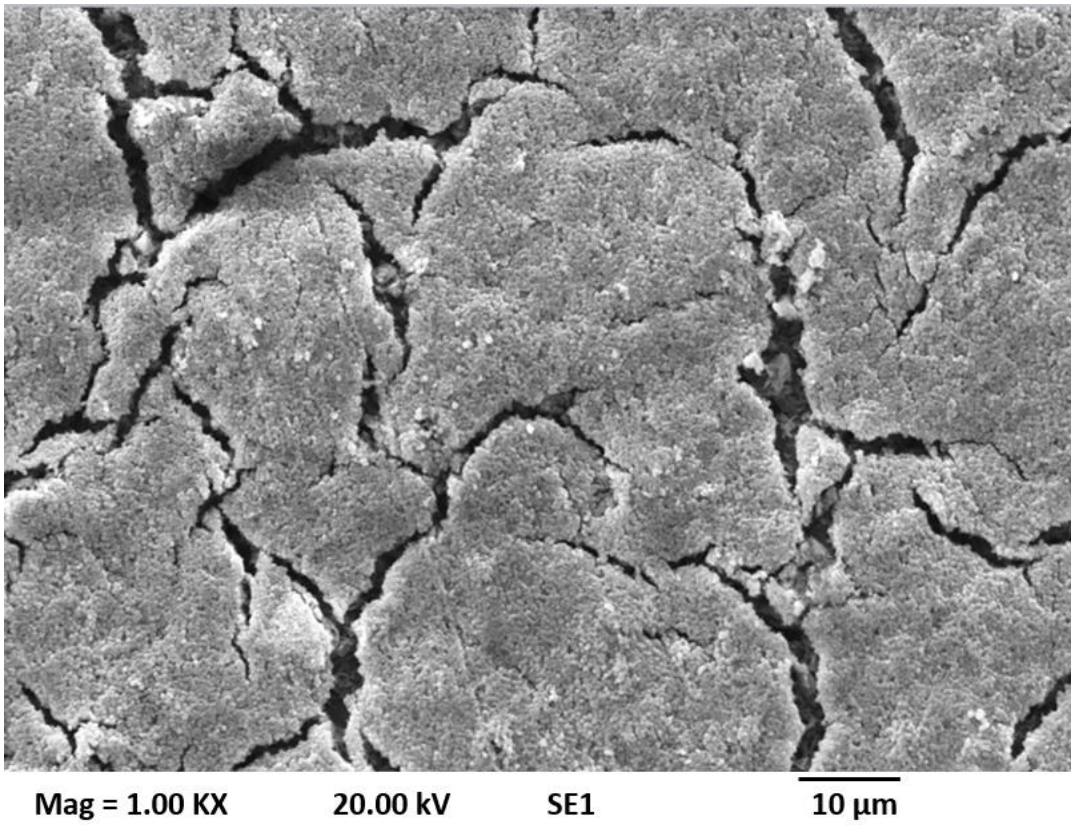

(f)

Figure 21: SEM of corrosion products formed on X65 carbon steel at 50°C in (a) 1 wt. % NaCl, 7 h, (b) 1 wt. % NaCl, 168 h (c) 3.5 wt. % NaCl , 7 h (d) 3.5 wt. % NaCl, 168 h, (e) 10wt. % NaCl, 7 h, and (f) 10 wt. % NaCl solutions, 168 h.

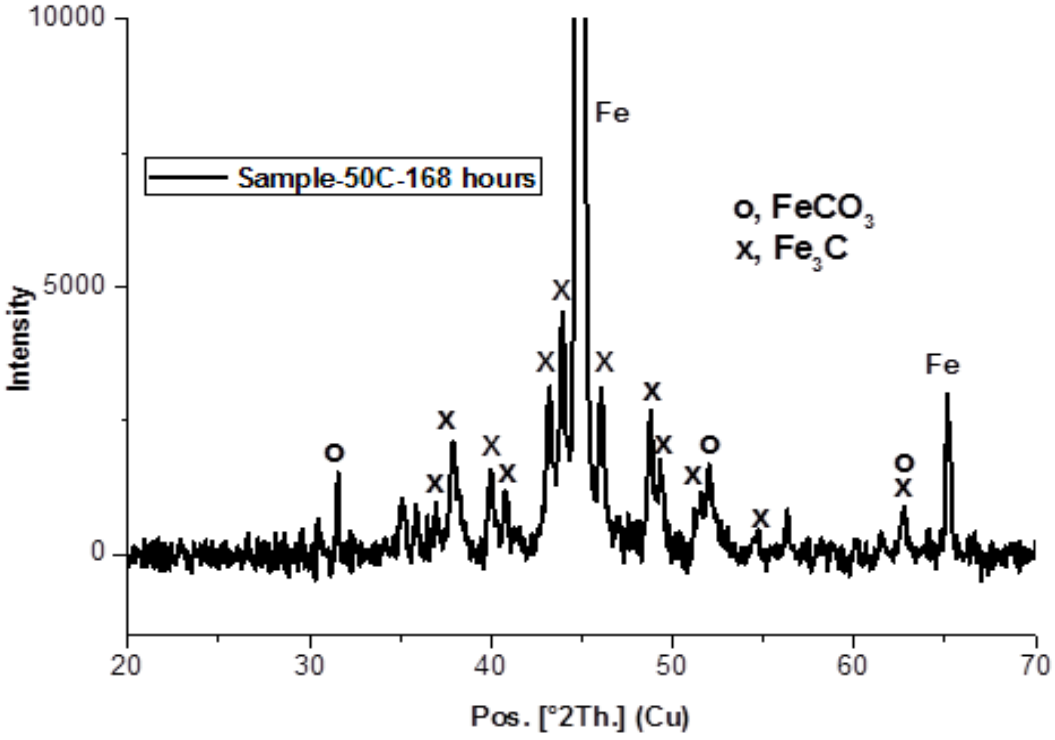

(a)

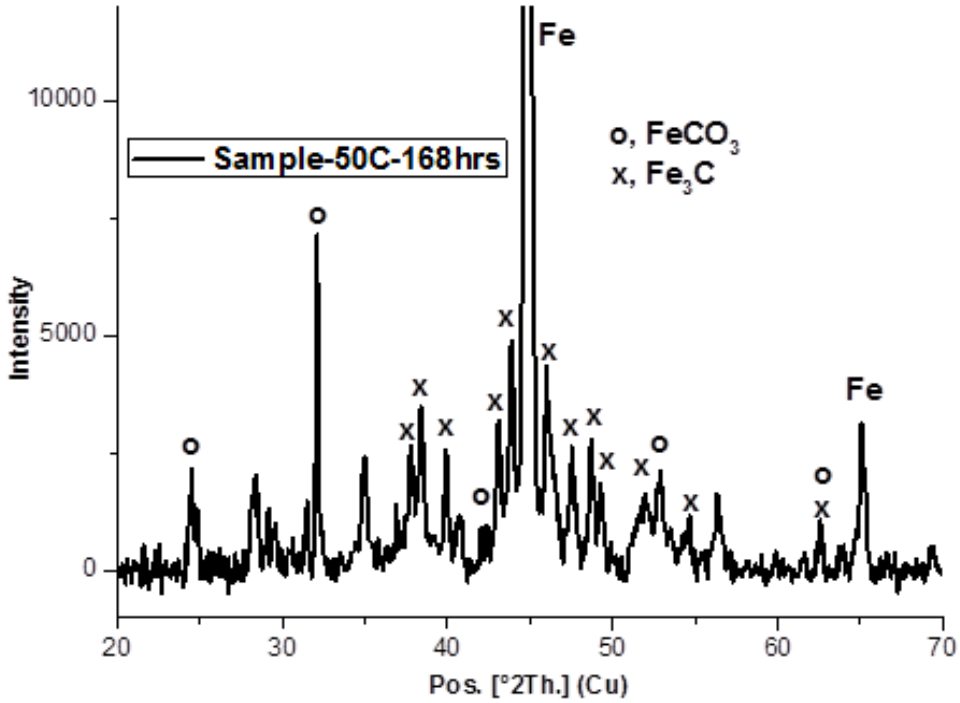

(b)

Figure 22: XRD patterns for (a) 1 wt. % and (b) 10 wt. % NaCl solutions for 168 h at 50°C (Note that the intensity scale is arbitrary). XRD patterns are referenced to the literature [33-36].

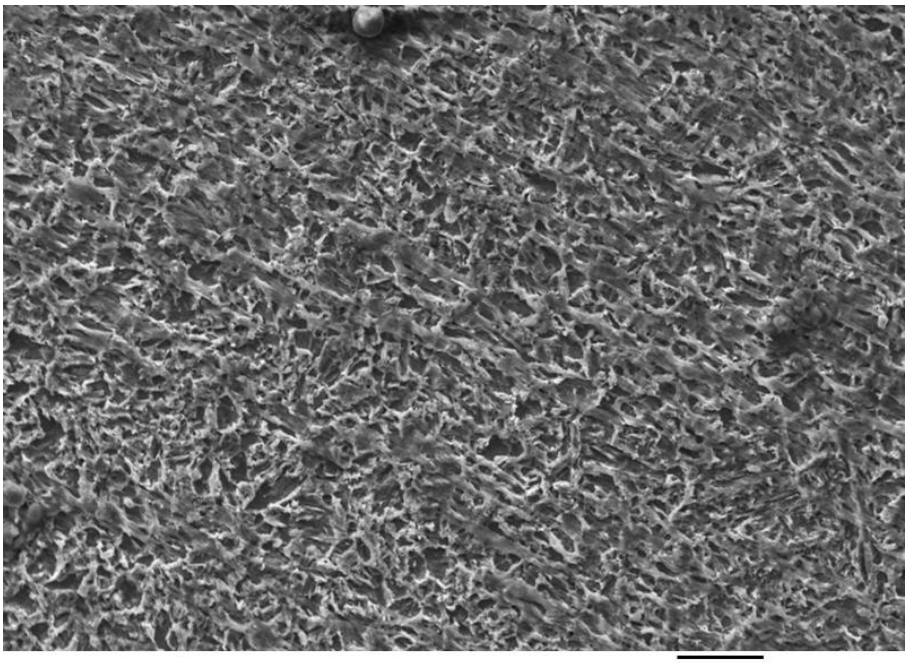

(a)

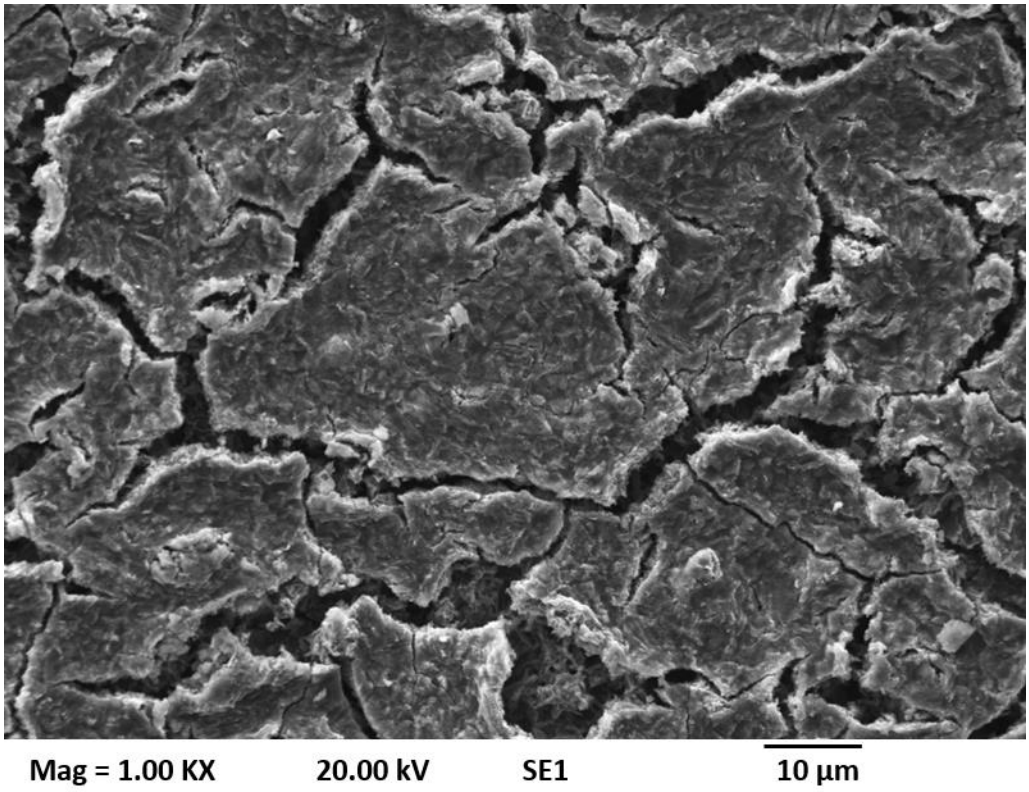

(b)

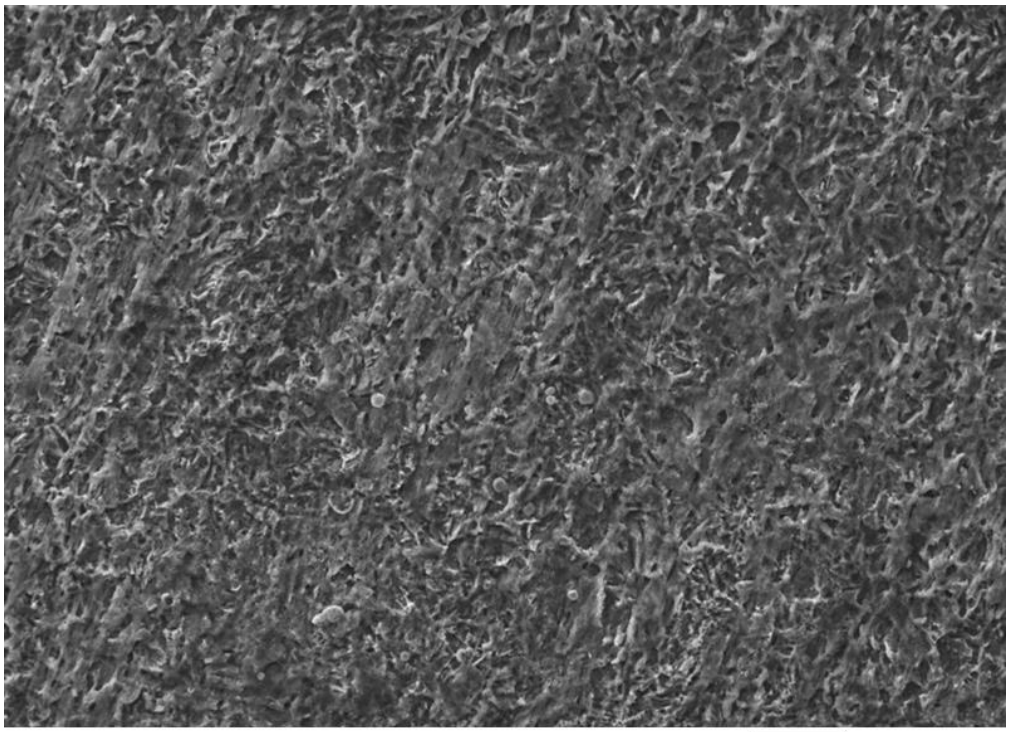

(c)

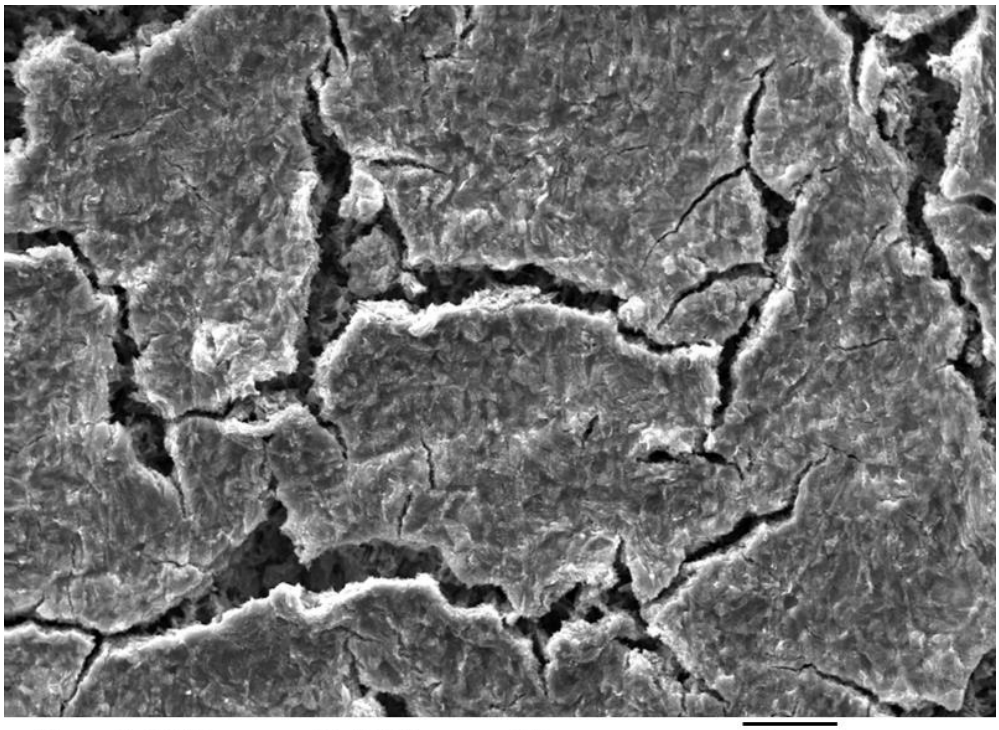

(d)

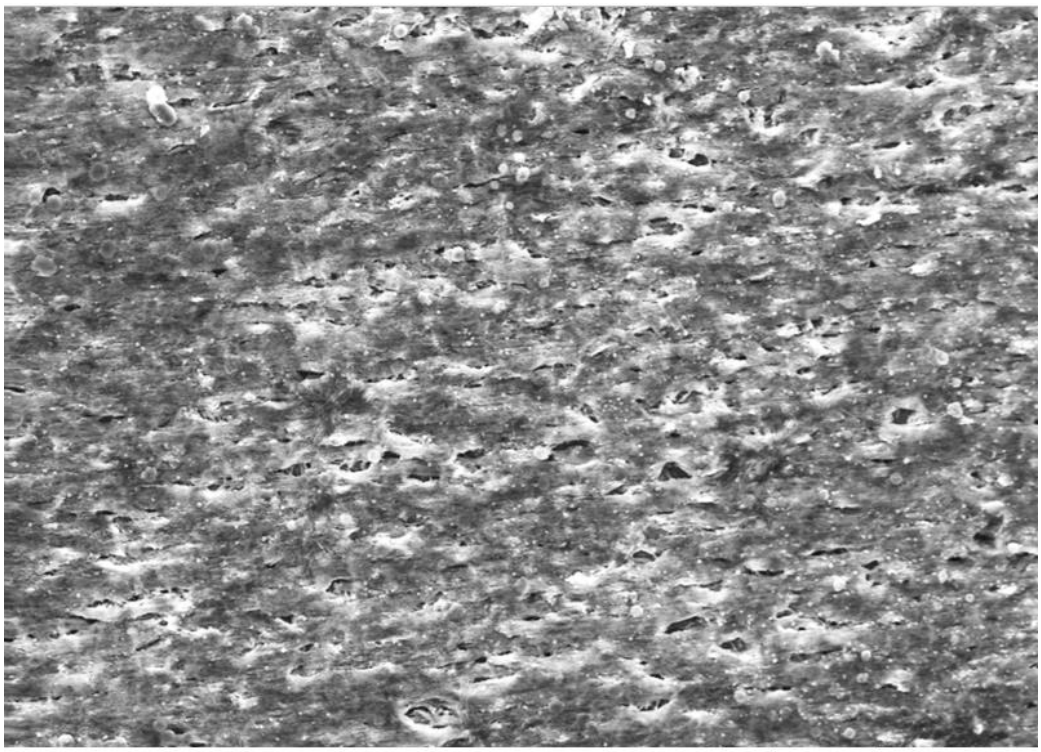

(e)

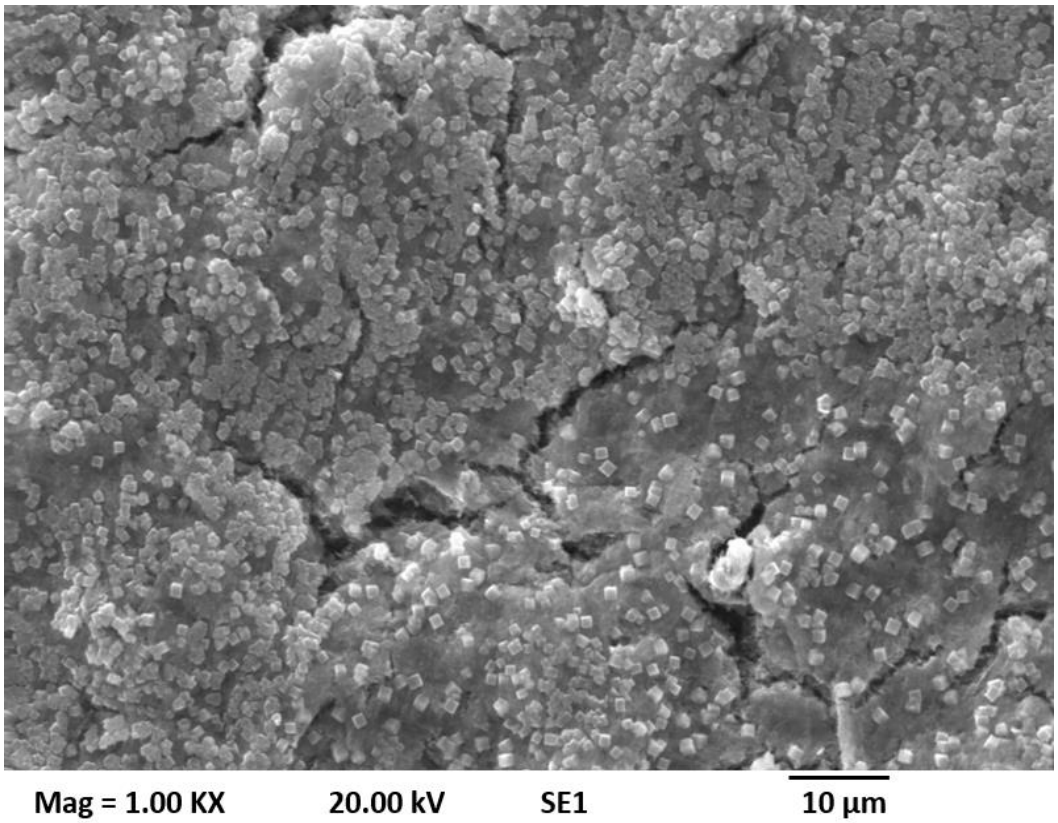

(f)

Figure 23: SEM of corrosion products formed on X65 carbon steel at 80°C in (a) 1 wt. % NaCl, 7 h, (b) 1 wt. % NaCl, 168 h (c) 3.5 wt. % NaCl, 7 h (d) 3.5 wt. % NaCl, 168 h, (e) 10wt. % NaCl, 7 h, and (f) 10 wt. % NaCl, 168 h.

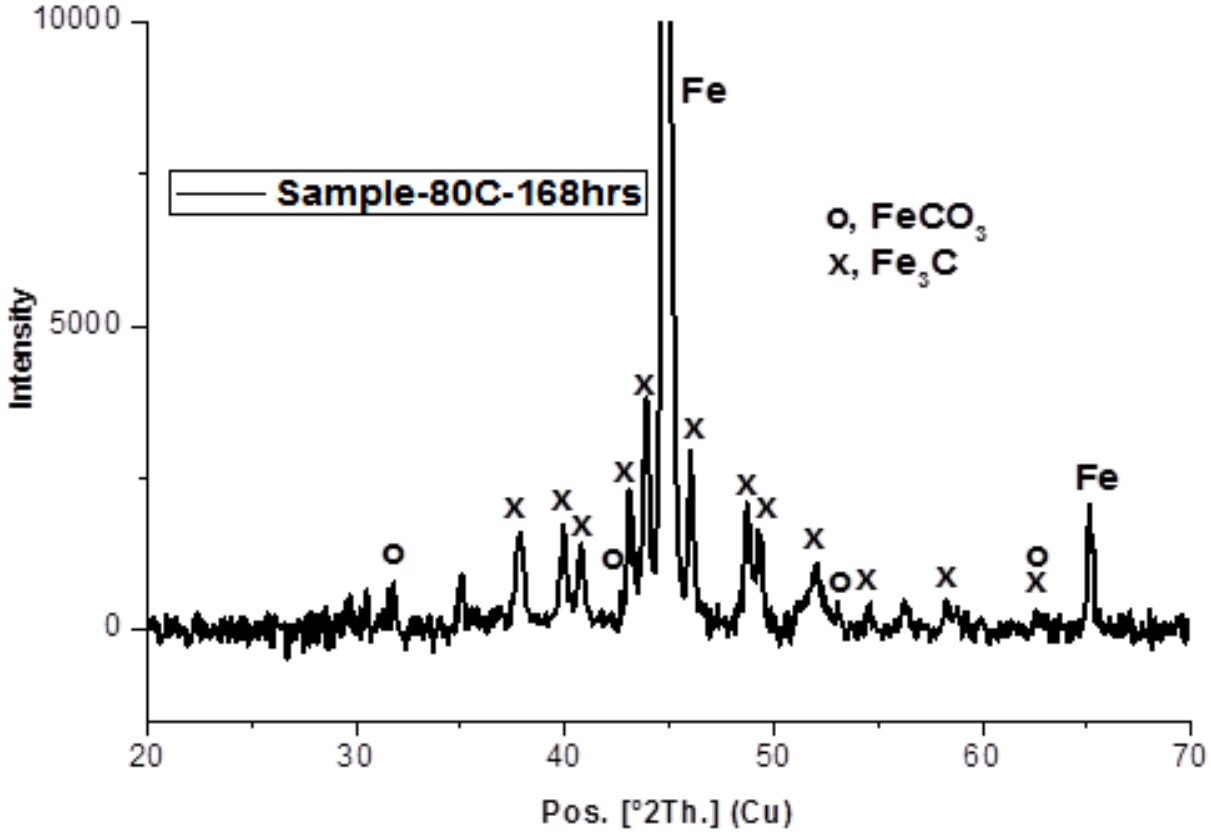
10000
5000
0
Intensity
Sample-80C-168hrs
Fe
o, FeCO3
x, Fe3C
Fe
20
30
40
50
60
70
Pos. [°2Th.] (Cu)

(a)

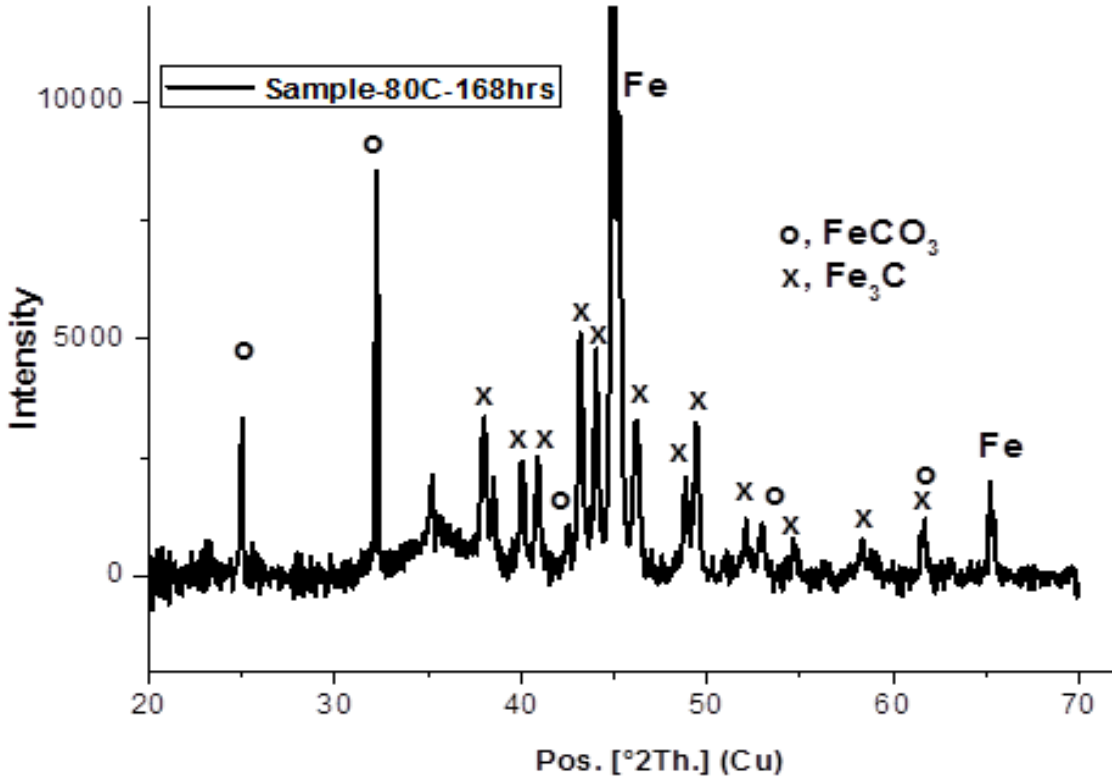
10000
5000
0
Intensity
Sample-80C-168hrs
Fe
o, FeCO3
x, Fe3C
Fe
20
30
40
50
60
70
Pos. [°2Th.] (Cu)

(b)

Figure 24: XRD patterns for (a) 1 wt. % and (b) 10 wt. % NaCl solutions for 168 h at 80°C (Note that the intensity scale is arbitrary). XRD patterns are referenced to the literature [33-36].

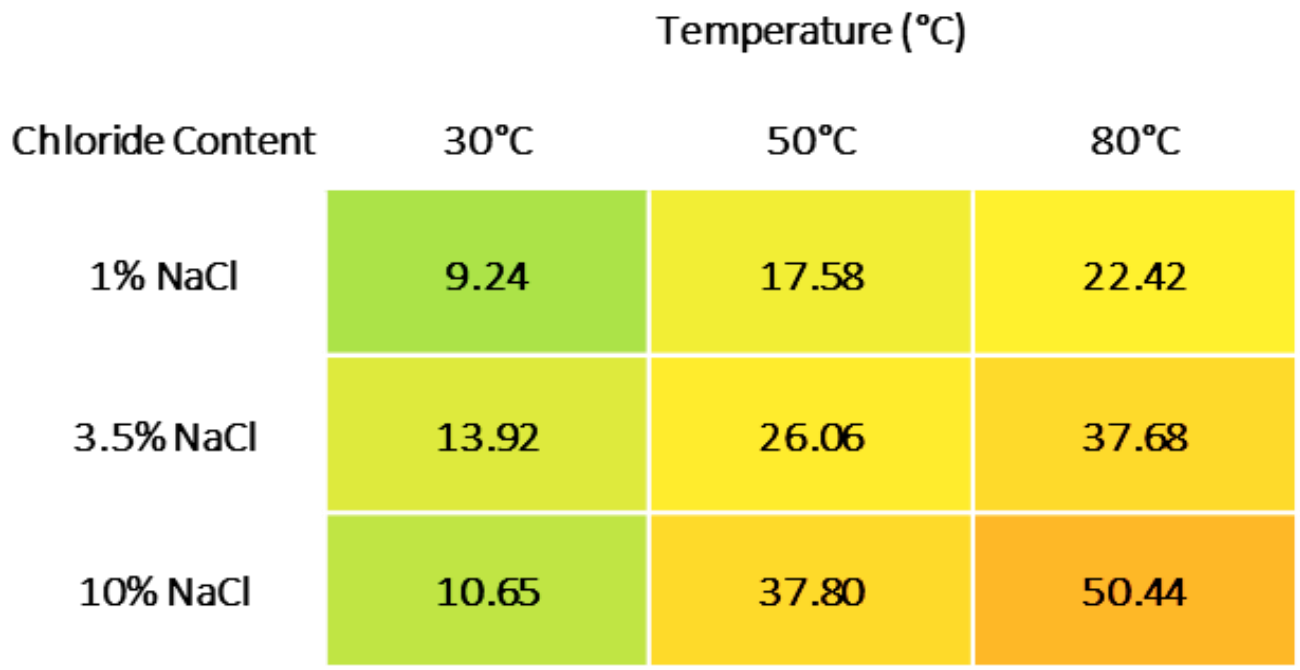

(a)

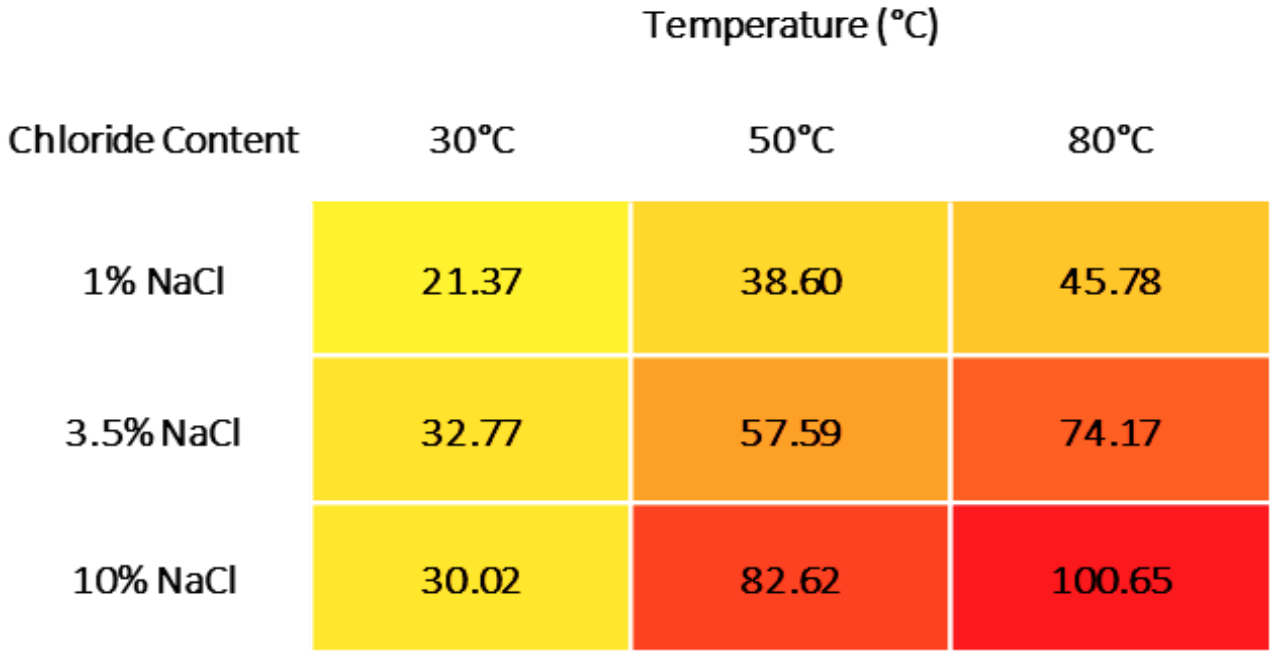

(b)

Figure 25: Estimated thickness loss (µm) based on LPR measurements showing the synergistic effect of chloride ion concentration and temperature on carbon steel penetration after (a) 72 h and (b) 168 h. *Note: severity of material loss in magnitude increases in this order; Green → Amber → Red.*

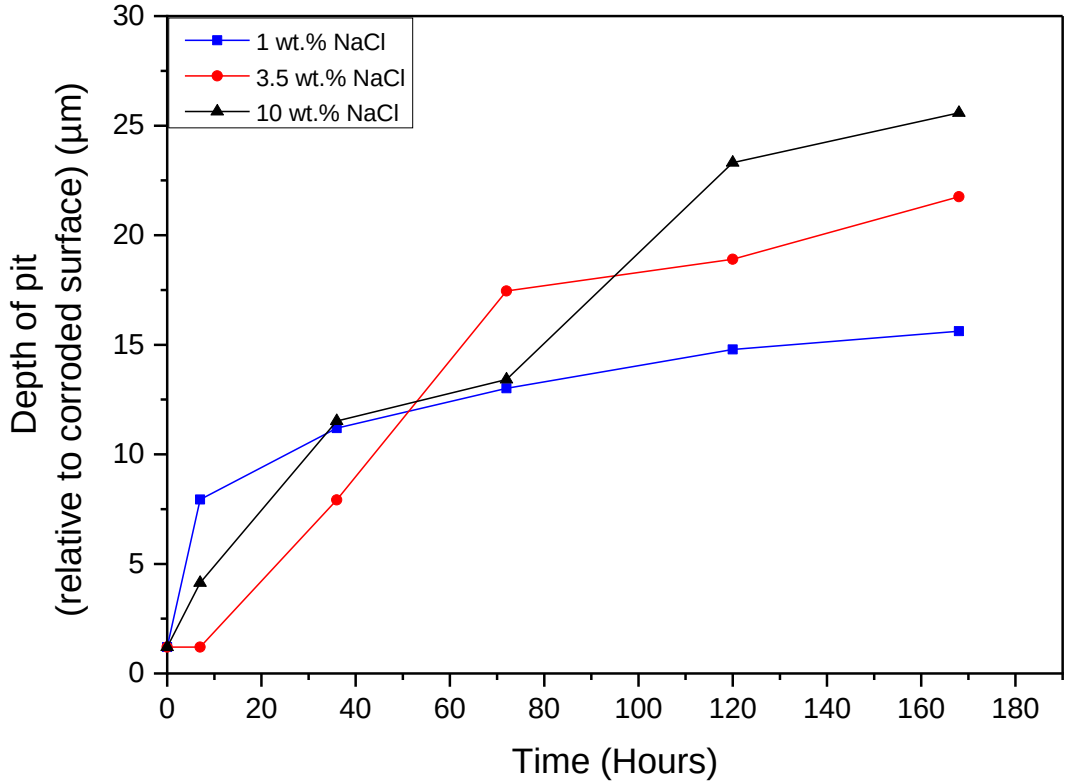
1 wt.% NaCl
3.5 wt.% NaCl
10 wt.% NaCl
Depth of pit
(relative to corroded surface) (µm)
Time (Hours)
0
5
10
15
20
25
30
0
20
40
60
80
100
120
140
160
180

(a)

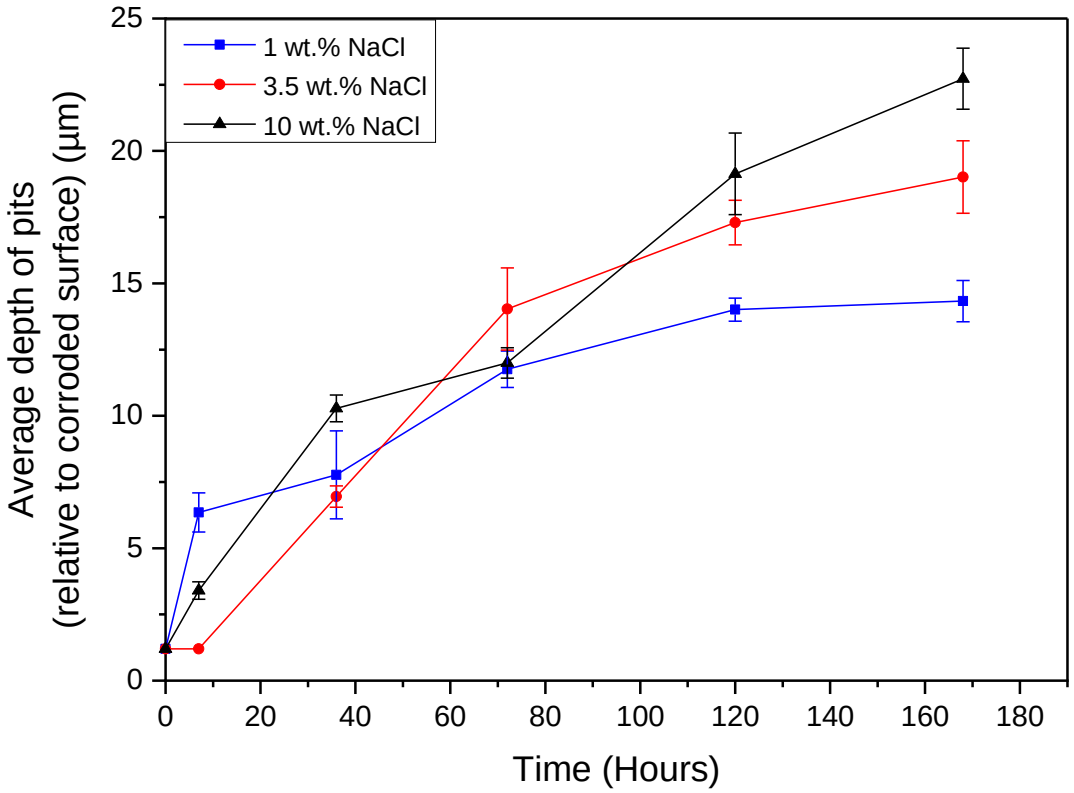
1 wt.% NaCl
3.5 wt.% NaCl
10 wt.% NaCl
Average depth of pits
(relative to corroded surface) (µm)
Time (Hours)
0
5
10
15
20
25
0
20
40
60
80
100
120
140
160
180

(b)

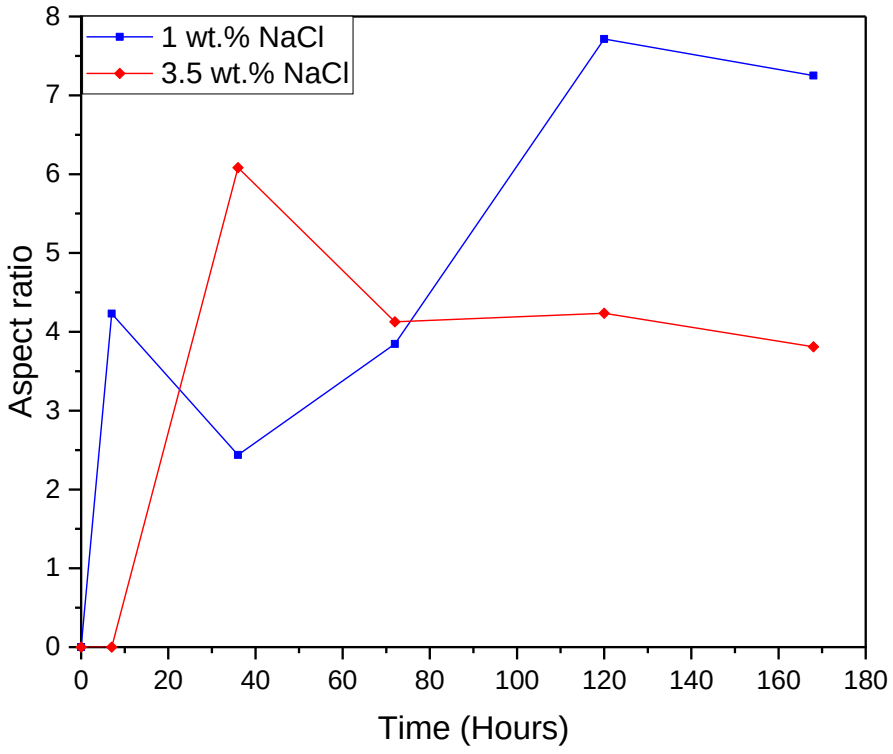

(c)

Figure 26: Pitting corrosion in X65 carbon steel in different NaCl solutions over 168 h, at 30°C (a) Deepest pit, (b) average depth of pits and (c) Aspect ratio based on the diameter of deepest pit. ***Note: Pit depth quantified after removal of corrosion product layer and Error bars on average depth of pits represents the standard deviation of 10 deepest pits.***

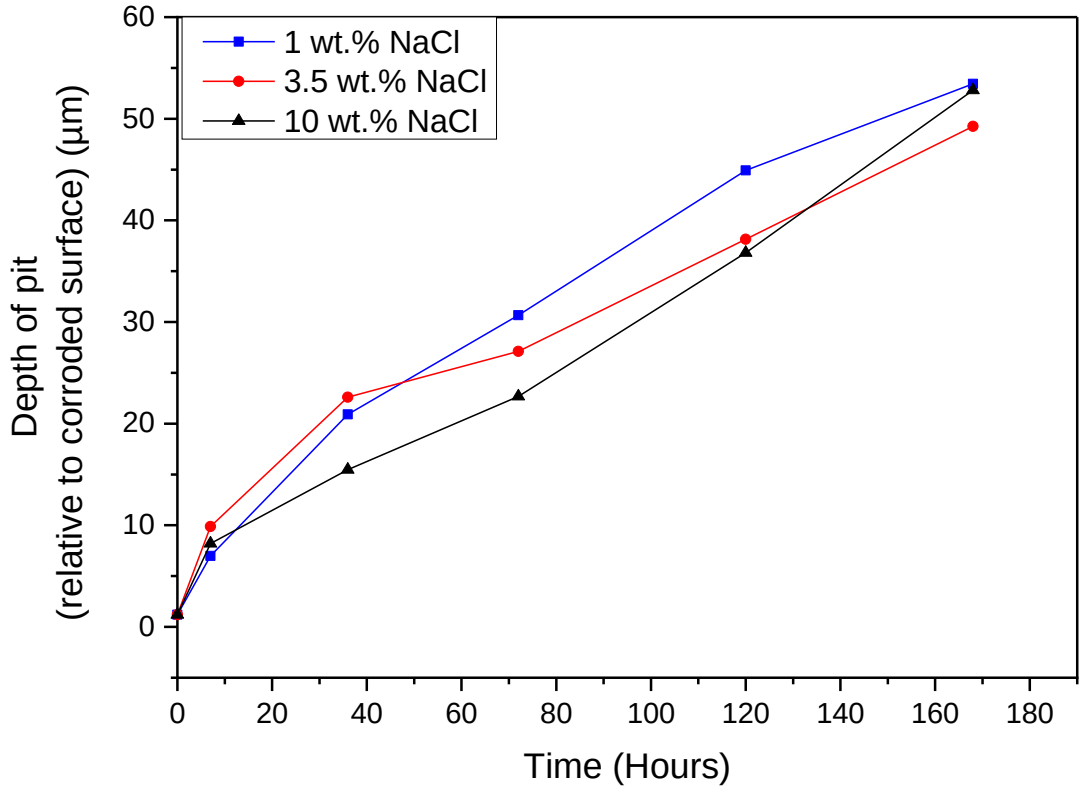

(a)

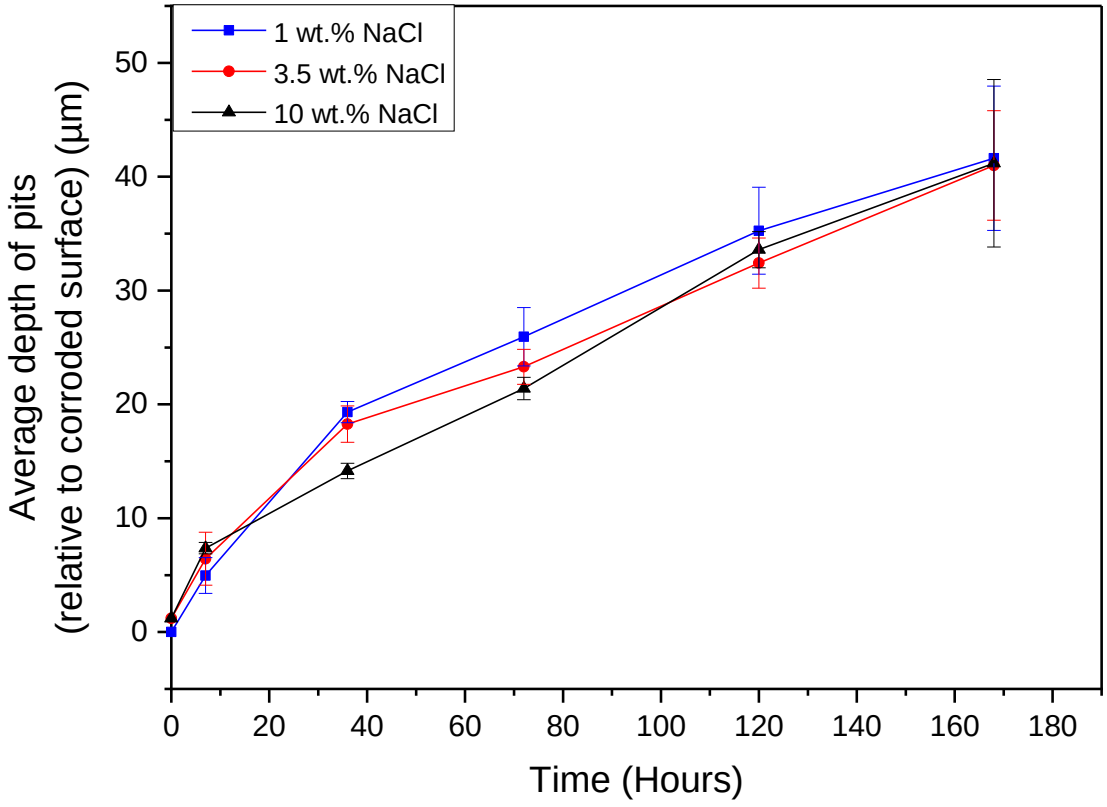

(b)

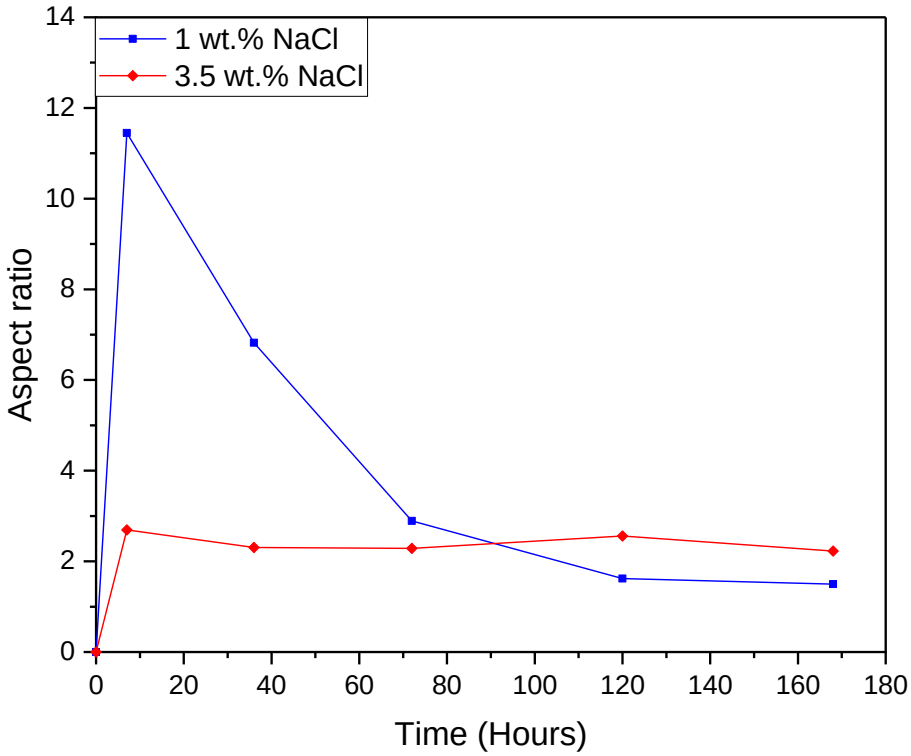

(c)

Figure 27 : Pitting corrosion in X65 carbon steel in different NaCl solutions over 168 h, at 50°C (a) Deepest pit, (b) average depth of pits and (c) Aspect ratio based on the diameter of deepest pit. ***Note: Pit depth quantified after removal of corrosion product layer and Error bars on average depth of pits represents the standard deviation of 10 deepest pits.***

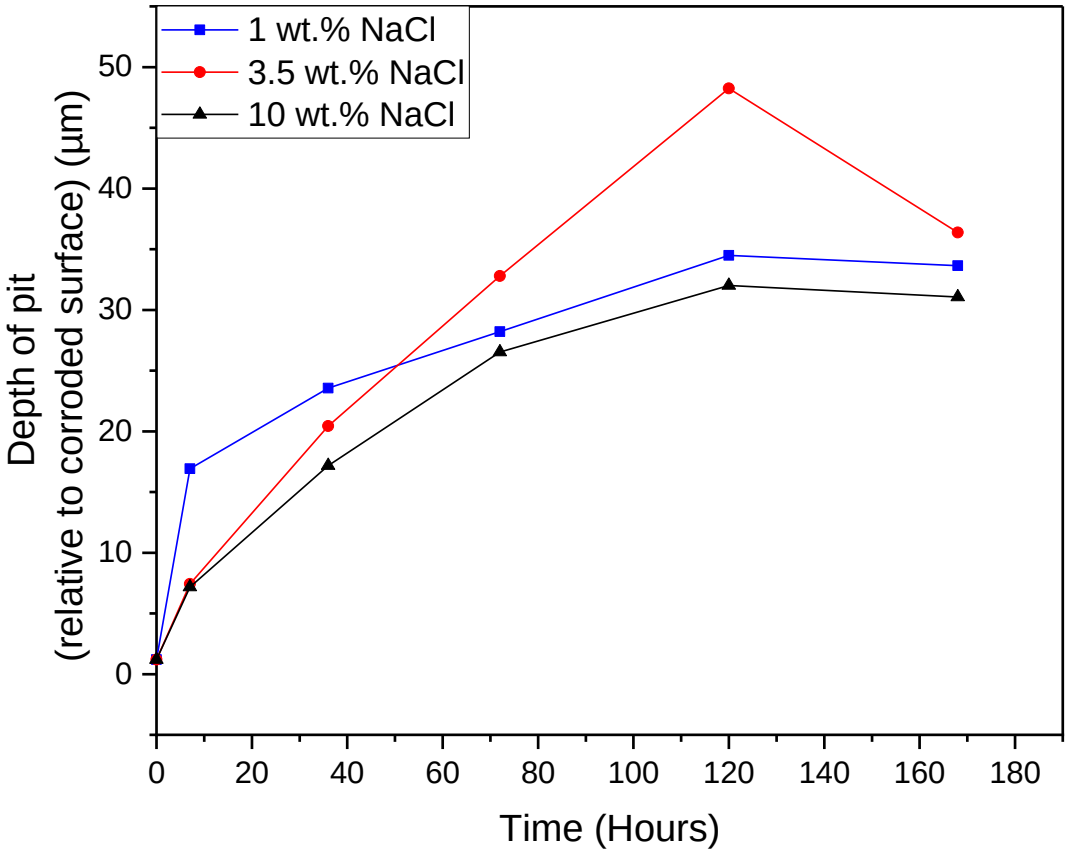
1 wt.% NaCl
3.5 wt.% NaCl
10 wt.% NaCl
Depth of pit
(relative to corroded surface) (µm)
0
10
20
30
40
50
0
20
40
60
80
100
120
140
160
180
Time (Hours)

(a)

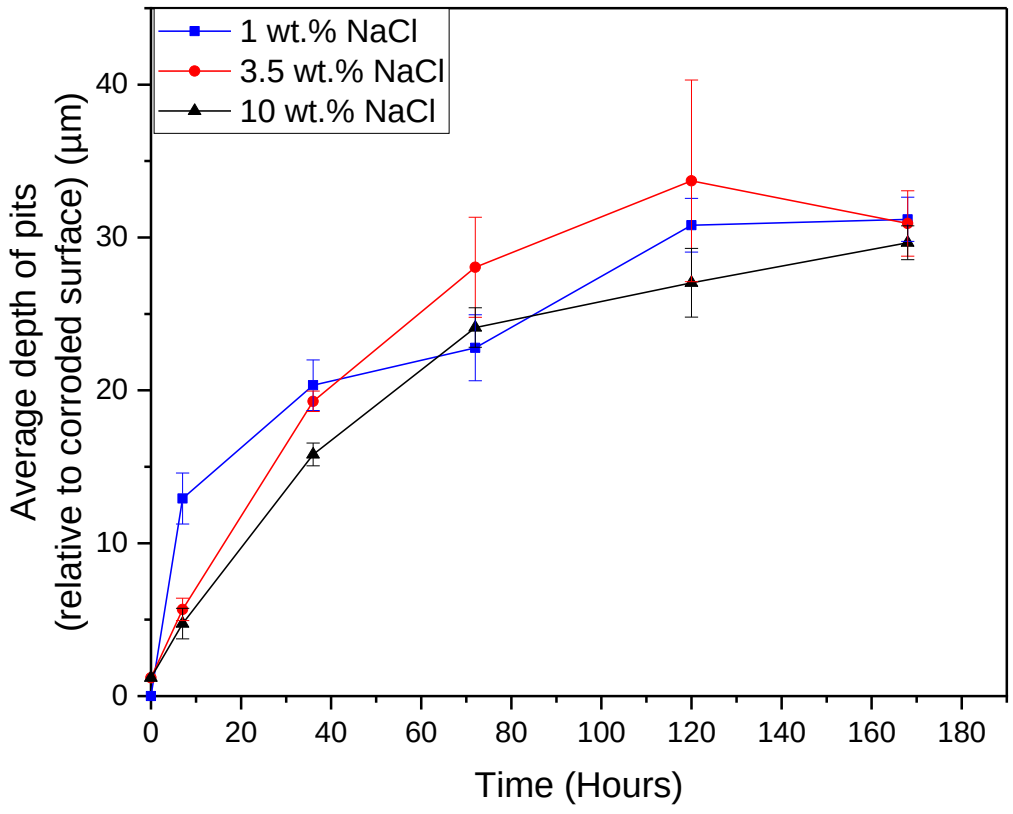
1 wt.% NaCl
3.5 wt.% NaCl
10 wt.% NaCl
Average depth of pits
(relative to corroded surface) (µm)
0
10
20
30
40
0
20
40
60
80
100
120
140
160
180
Time (Hours)

(b)

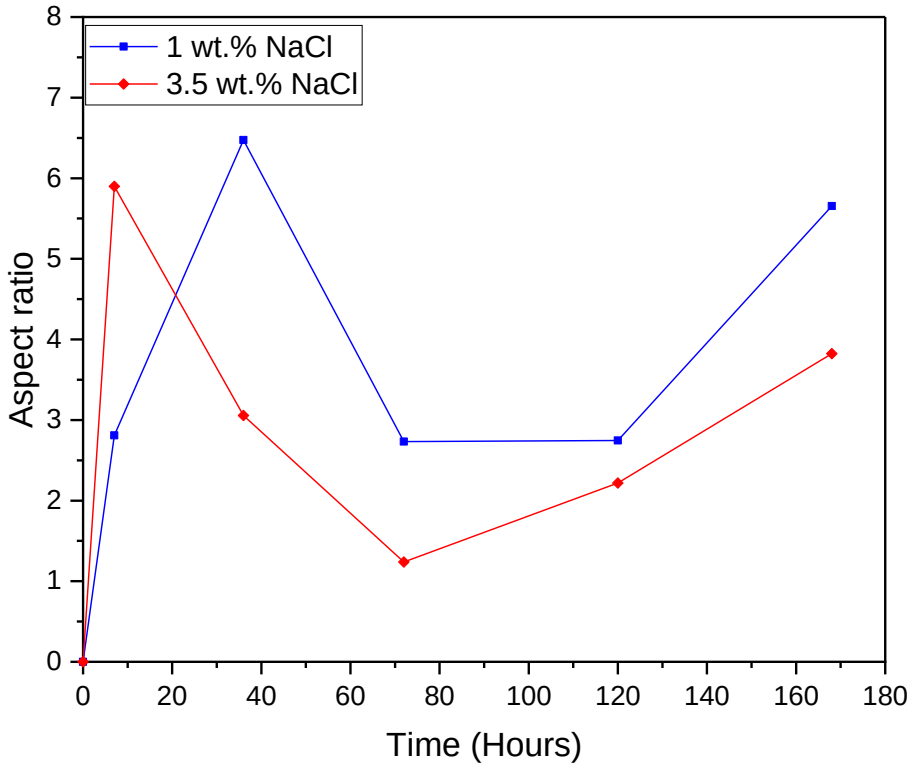

(c)

Figure 28: Pitting corrosion in X65 carbon steel in different NaCl solutions over 168 h, at 80°C (a) Deepest pit, (b) average depth of pits and (c) Aspect ratio based on the diameter of deepest pit. ***Note: Pit depth quantified after removal of corrosion product layer and Error bars on average depth of pits represents the standard deviation of 10 deepest pits.***

Chloride Content	Temperature (°C) 30°C	50°C	80°C
1% NaCl	22.26	48.25	50.62
3.5% NaCl	31.37	53.16	70.49
10% NaCl	24.07	60.47	76.96

(a)

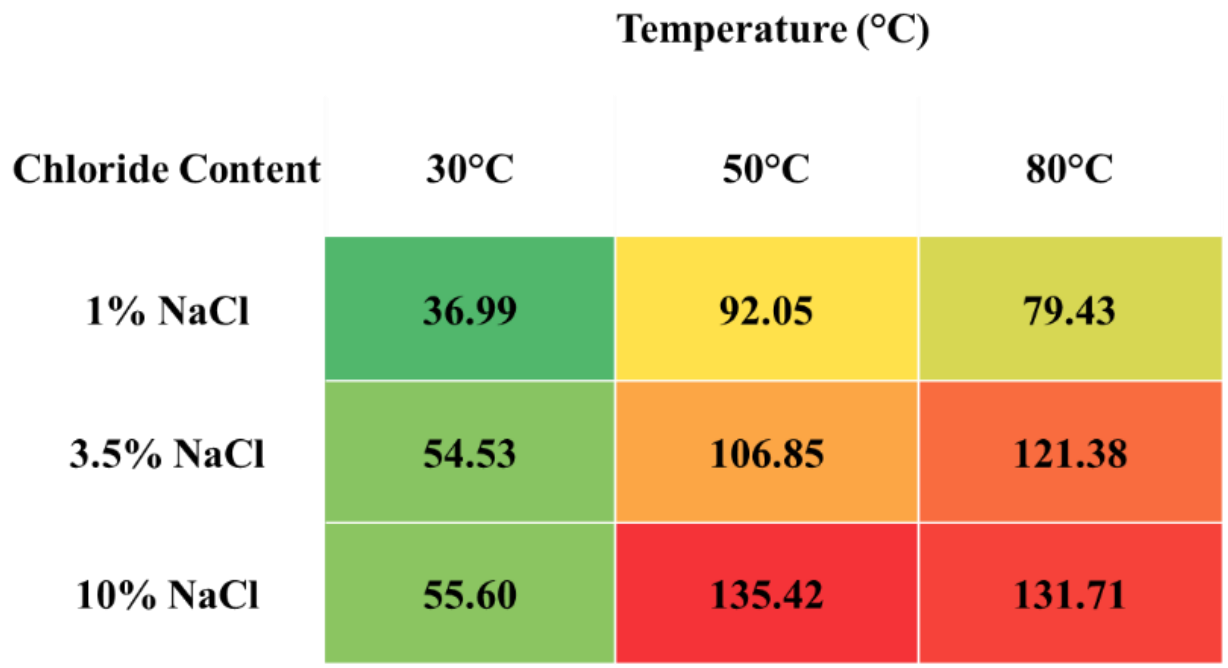

(b)

Figure 29: Matrix to qualify the effect of synergy of chloride ion concentration and temperature on total metal penetration of carbon steel after (a) 72 h and (b) 168 h. ***Note: severity of material loss in magnitude increases in this order; Green → Amber → Red.***

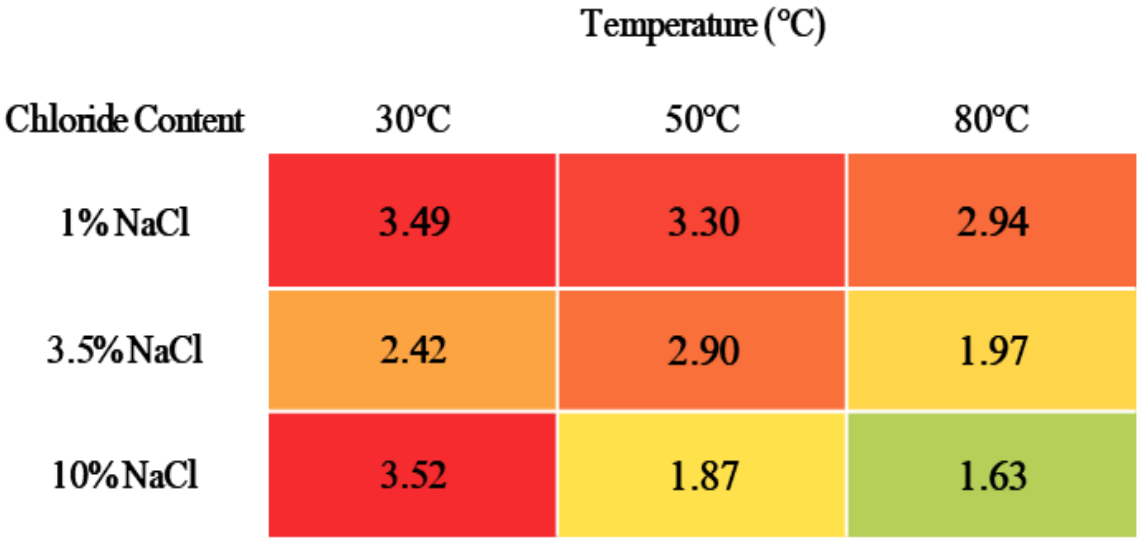

(a)

Temperature (°C)

Chloride Content	30°C	50°C	80°C
1% NaCl	2.41	2.74	2.26
3.5% NaCl	2.25	2.04	1.87
10% NaCl	2.26	1.60	1.53

(b)

Temperature (°C)

Chloride Content	30°C	50°C	80°C
1% NaCl	1.73	2.38	1.74
3.5% NaCl	1.67	1.86	1.49
10% NaCl	1.85	1.64	1.31

(c)

Figure 30: Matrix to qualify the effect of synergy of chloride ion concentration and temperature on the contribution to metal penetration from both pitting and uniform corrosion in terms of pitting factor on carbon steel after (a) 36 h, (b) 72 h and (c) 168 h. ***Note: severity of material loss in magnitude increases in this order; Green → Amber → Red.***